



Article

Functional Studies of Deafness-Associated Pendrin and Prestin Variants

Satou Takahashi ¹ , Takashi Kojima ^{1,2}, Koichiro Wasano ^{1,3} and Kazuaki Homma ^{1,4,*}

¹ Department of Otolaryngology—Head and Neck Surgery, Feinberg School of Medicine, Northwestern University, Chicago, IL 60611, USA

² Department of Otolaryngology, Head and Neck Surgery, National Hospital Organization Tochigi Medical Center, Tochigi 320-0057, Japan

³ Department of Otolaryngology, Head and Neck Surgery, Tokai University School of Medicine, Isehara 259-1193, Japan

⁴ The Hugh Knowles Center for Clinical and Basic Science in Hearing and Its Disorders, Northwestern University, Evanston, IL 60208, USA

* Correspondence: k-homma@northwestern.edu; Tel.: +1-312-503-5344

Abstract: Pendrin and prestin are evolutionary-conserved membrane proteins that are essential for normal hearing. Dysfunction of these proteins results in hearing loss in humans, and numerous deafness-associated pendrin and prestin variants have been identified in patients. However, the pathogenic impacts of many of these variants are ambiguous. Here, we report results from our ongoing efforts to experimentally characterize pendrin and prestin variants using in vitro functional assays. With previously established fluorometric anion transport assays, we determined that many of the pendrin variants identified on transmembrane (TM) 10, which contains the essential anion binding site, and on the neighboring TM9 within the core domain resulted in impaired anion transport activity. We also determined the range of functional impairment in three deafness-associated prestin variants by measuring nonlinear capacitance (NLC), a proxy for motor function. Using the results from our functional analyses, we also evaluated the performance of AlphaMissense (AM), a computational tool for predicting the pathogenicity of missense variants. AM prediction scores correlated well with our experimental results; however, some variants were misclassified, underscoring the necessity of experimentally assessing the effects of variants. Together, our experimental efforts provide invaluable information regarding the pathogenicity of deafness-associated pendrin and prestin variants.

Keywords: pendrin; SLC26A4; prestin; SLC26A5; pendred syndrome; DFNB4; DFNB61; hereditary hearing loss; nonlinear capacitance



Citation: Takahashi, S.; Kojima, T.; Wasano, K.; Homma, K. Functional Studies of Deafness-Associated Pendrin and Prestin Variants. *Int. J. Mol. Sci.* **2024**, *25*, 2759. <https://doi.org/10.3390/ijms25052759>

Academic Editor: Francesco Pallotti

Received: 30 January 2024

Revised: 21 February 2024

Accepted: 23 February 2024

Published: 27 February 2024



Copyright: © 2024 by the authors. Licensee MDPI, Basel, Switzerland. This article is an open access article distributed under the terms and conditions of the Creative Commons Attribution (CC BY) license (<https://creativecommons.org/licenses/by/4.0/>).

1. Introduction

The SLC26 family of membrane proteins includes two members, pendrin (SLC26A4) and prestin (SLC26A5), that are essential for normal hearing. Pendrin is an anion transporter required for normal development and maintenance of ion homeostasis in the inner ear [1,2]. Prestin is a voltage-dependent motor and mediates voltage-dependent somatic motility (electromotility) of cochlear outer hair cells (OHCs), which is essential for the high sensitivity and frequency selectivity of mammalian hearing [3–6]. Dysfunction or loss of these SLC26 proteins results in hearing loss. Pendrin-coding *SLC26A4* is a causative gene for Pendred syndrome (PDS, OMIM 274600), which is one of the most common types of syndromic hearing loss with enlarged vestibular aqueduct (EVA) and goiter, as well as nonsyndromic hearing loss (DNFB4, OMIM600791) [7,8]. Prestin-coding *SLC26A5* is associated with nonsyndromic hearing loss (DNFB61, OMIM613865). Since the advent of next-generation sequencing, a large number of deafness-associated variants have been identified in patients. As of January 2024, 704 and 16 variants have been identified in *SLC26A4* and *SLC26A5*, respectively (The Human Gene Mutation Database [9]). However,

experimental assessments of the functional phenotypes of these genetic variants have been lagging behind in determining their pathogenicity with confidence. Previously, we quantitated the anion transport functions of disease-associated pendrin variants in order to understand the pathology underlying the various severity of PDS and DFNB4 [10]. Similarly, we characterized the functional phenotypes of prestin variants both in vitro and in vivo to determine their pathogenicity [11,12]. Those experimental efforts are indispensable to providing information regarding the effects of variants on protein functions, which in turn improves the consistency and accuracy in genetic diagnoses of patients. This is in line with the American College of Medical Genetics and Genomics (ACMG) and the Association for Molecular Pathology (AMP) guidelines for the interpretation of sequence variants adapted for genetic hearing loss [13].

In this study, we continue to assess the pathogenicity of deafness-associated pendrin and prestin variants in vitro to determine their roles in hearing loss in patients. For pendrin, highly reproducible fluorometric antiport assays previously developed by our group were used to interrogate the functional impacts of pendrin variants on the anion transport function [10], with a major focus on transmembrane (TM) 9 and 10 located within the core domain that accommodates an anion substrate and undergoes elevator-like motions with respect to the gate domain during the transport cycle. Since the number of variants identified was clustered around this functionally important region, we reasoned that the likelihood of identifying the pathogenic variants would be high. For prestin, nonlinear capacitance (NLC) measurement was used to determine the functional impacts of a few prestin variants reported to date on the motile function [14,15]. In addition, we compared our experimental results with predictions from AlphaMissense (AM) [16], a recently developed in silico tool that predicts variant effects using artificial intelligence. We found a decent correlation between AM pathogenicity scores and the antiport activity of pendrin variants, indicating good overall performance of this prediction tool ($r = -0.6497$). However, some of the variants were miscategorized, indicating that prediction tools still have limitations and that experimental efforts remain important to assess the pathogenicity of deafness-associated variants.

2. Results

2.1. Functional Characterization of Pendrin Variants

A recent cryo-EM study on mouse pendrin [17] revealed a homodimeric architecture that is similar to prestin [18–21] and other SLC26 proteins [22–24]. The transmembrane domain consists of the gate and the core domains, and the ion translocation pathway is located in between them (Figure 1A). The positive helix dipoles of TM3 and TM10 (their N-termini), together with a conserved basic residue (Arg⁴⁰⁹ and Arg³⁹⁹ in pendrin and prestin, respectively) in TM10, constitute a positively charged pocket that holds a variety of anion substrates. The N-terminus of TM10 is connected to TM9, which is located on the opposite side of the core domain. The importance of the conserved residues in TM9, TM10, and the linker portion connecting these two helices (Figure 1B) is suggested by the presence of multiple clustered missense variants identified in these regions: p.D380N (c.1138G>A), p.N382K (c.1146C>G), p.Q383E (c.1147C>G), p.Q383P (c.1148A>C), p.E384Q (c.1150G>C), p.E384G (c.1151A>G), p.I386V (c.1156A>G), p.A387V (c.1160C>T), p.G389R (c.1165G>A), p.G389R (c.1165G>C), p.S391R (c.1173C>A), p.S391N (c.1172G>A), p.N392S (c.1175A>G), p.N392Y (c.1174A>T), p.G396E (c.1187G>A), p.S399P (c.1195T>C), p.V402L (c.1204G>T), p.V402M (c.1204G>A), p.T404N (c.1211C>A), p.T404I (c.1211C>T), p.A406T (c.1216G>A), p.R409C (c.1225C>T), p.R409H (c.1226G>A), p.R409L (c.1226G>T), p.R409P (c.1226G>C), p.T410K (c.1229C>A), p.T410M (c.1229C>T), p.A411P (c.1231G>C), p.A411T (c.1231G>A), p.V412I (c.1234G>A), p.Q413R (c.1238A>G), p.Q413P (c.1238A>C), p.E414K (c.1240G>A), p.S415R (c.1245C>A), p.S415G (c.1243A>G), p.T416P (c.1246A>C) [10,25–54]. Among them, p.E384G, p.N392Y, p.S399P, p.R409H, p.T410K, p.T410M, p.Q413R, p.Q413P, and p.T416P were functionally characterized and found to significantly impair the anion transport function of pendrin in previous studies by us and others [10,42,55–61]. The

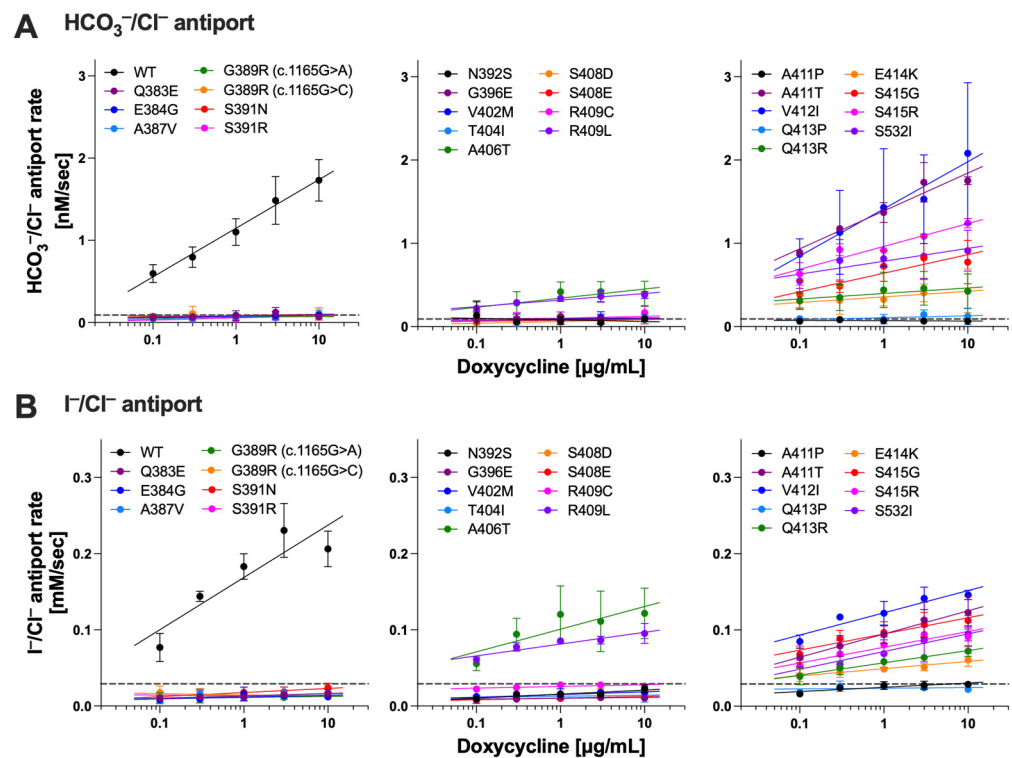


Figure 2. HCO₃⁻/Cl⁻ and I⁻/Cl⁻ antiport assays on pendrin variants. HCO₃⁻/Cl⁻ (A) and I⁻/Cl⁻ (B) antiport rates were plotted against doxycycline (Dox) concentration (0.1–10 µg/mL) for each mTq2-tagged pendrin variant alongside WT as indicated. Horizontal dotted lines indicate transport rates of uninduced cells. Error bars indicate SD. Solid lines indicate linear regressions (log₁₀ [Dox] vs. transport rates). Sample size information and statistics are provided in Table 1.

2.2. Functional Characterization of Prestin Variants

Mammalian prestin is unique among the SLC26 family of proteins as it functions as a voltage-dependent motor instead of a transporter. Prestin also shares the same overall similarities in structure as pendrin and other SLC26 proteins, implying a common molecular principle underlying transport and motor functions. Thus, it is conceivable that conserved residues between pendrin and prestin are of similar functional importance in these structurally similar proteins. Interestingly, however, the number of prestin missense variants reported to date is only 13, six of which are associated with autism with unknown pathophysiological relevance to hearing [54,62–68]. In this study, we characterized p.A100T (c.298G>A), p.P119S (c.355C>T), and p.S441L (c.1322C>T) prestin variants that are all associated with hearing loss. The locations of these three prestin missense variants are indicated in Figure 3A. We established HEK293T cell lines expressing these prestin variants and measured the NLC as a proxy for their motor function. Figure 4A shows the NLC of p.A100T and p.P119S prestin compared to WT. Although reduced, the NLC was detected for both p.A100T and p.P119S prestin, indicating some residual activity for these variants (Figure 4B). These Ala and Pro residues are relatively well conserved among the SLC26 proteins (Ala¹⁰⁴ and Pro¹²³, respectively, in pendrin, Figure 3B), and previous studies by us and others have shown that the p.P123S variant significantly impairs the anion transport function of pendrin [10,57]. In this study, we also measured the HCO₃⁻/Cl⁻ antiporter activity for p.A104V pendrin (deafness-associated) and p.A104T pendrin (equivalent to p.A100T prestin but not identified in patients as of January 2024) and found that these two pendrin missense variants also significantly impair the anion transport function (Figure 5, left), suggesting the common importance of these conserved residues for pendrin and prestin.

Unlike p.A100T and p.P119S, the NLC of p.S441L prestin was undetectable, indicating that p.S441L completely abrogates the motor function of prestin (Figure 4A,B). Ser⁴⁴¹ is located at the interface between the gate and core domains (Figure 3A, right). Equivalent residues at this site in the other SLC26 family members are either Ala or Gly (Ala⁴⁵¹ in pendrin). These small residues may be important not to hinder the relative elevator-like movements of the core domain with respect to the gate domain. If true, p.S441L may sterically interfere with these interdomain motions. In line with this speculation, p.A451L in pendrin (equivalent to p.S441L in prestin) abolished the anion transport activity, whereas p.A451S and p.A451G did not (Figure 5, right). We also found that p.S441A prestin has a WT-like NLC (Figure 4A,B). These observations suggest the common importance of having a small residue at the Ser⁴⁴¹ site in prestin and equivalent sites in the other SLC26 proteins.

Table 1. Summaries of the antiport rates of pendrin variants determined in this study. Numerical data from HCO₃⁻/Cl⁻ and I⁻/Cl⁻ antiport assays and for HCO₃⁻/Cl⁻ antiport assays are listed as indicated. P-values from one-way ANOVA with Fisher’s LSD tests compared to uninduced basal rates were listed below the mean ± SD values for each Dox concentrations. The numbers in the parentheses indicate the sample size. Comparison to WT was performed using the F-test on slope values as in our previous study [10]. Box with gray shades indicate statistically not significant (p ≥ 0.05). Asterisks (*) indicate variants not found in human patients (as of January 2024).

	Transport Activity [Mean ± SD (n)]						Dox-Dependence Transport Activity/ log ₁₀ [Dox] (Slope ± SE)	Comparison to WT (F-Test)
	Dox: 0.1 µg/mL	Dox: 0.3 µg/mL	Dox: 1 µg/mL	Dox: 3 µg/mL	Dox: 10 µg/mL	Dox: 10 µg/mL		
WT	HCO ₃ ⁻ /Cl ⁻ [nM/sec]	0.597 ± 0.109 (10) p < 0.0001	0.795 ± 0.125 (10) p < 0.0001	1.102 ± 0.163 (10) p < 0.0001	1.485 ± 0.290 (10) p < 0.0001	1.731 ± 0.253 (10) p < 0.0001	0.591 ± 0.040 p < 0.0001	not applicable
	I ⁻ /Cl ⁻ [mM/sec]	0.08 ± 0.04 (3) p = 0.049	0.14 ± 0.01 (3) p = 0.0002	0.18 ± 0.02 (3) p < 0.0001	0.23 ± 0.04 (3) p < 0.0001	0.21 ± 0.02 (3) p < 0.0001	0.069 ± 0.012 p < 0.0001	not applicable
p.Gln383Glu (c.1147C>G)	HCO ₃ ⁻ /Cl ⁻ [nM/sec]	0.061 ± 0.023 (4) p = 0.4446	0.072 ± 0.029 (4) p = 0.6253	0.084 ± 0.060 (4) p = 0.8678	0.125 ± 0.059 (3) p = 0.3807	0.073 ± 0.020 (4) p = 0.6457	0.015 ± 0.014 p = 0.0034	Function impaired p < 0.0001
	I ⁻ /Cl ⁻ [mM/sec]	0.01 ± 0.003 (3) p = 0.2067	0.012 ± 0.003 (3) p = 0.2589	0.011 ± 0.004 (3) p = 0.2398	0.015 ± 0.001 (3) p = 0.3427	0.017 ± 0.005 (3) p = 0.4135	0.003 ± 0.001 p < 0.0001	Function impaired p < 0.0001
p.Glu384Gly (c.1151G>C)	HCO ₃ ⁻ /Cl ⁻ [nM/sec]	0.055 ± 0.018 (4) p = 0.2875	0.063 ± 0.028 (4) p = 0.407	0.081 ± 0.025 (4) p = 0.7755	0.088 ± 0.018 (4) p = 0.9276	0.081 ± 0.038 (4) p = 0.7679	0.016 ± 0.008 p = 0.066	Function impaired p < 0.0001
	I ⁻ /Cl ⁻ [mM/sec]	0.008 ± 0.002 (3) p = 0.1742	0.009 ± 0.002 (3) p = 0.1931	0.016 ± 0.009 (3) p = 0.3773	0.013 ± 0.004 (3) p = 0.3016	0.012 ± 0.002 (3) p = 0.2592	0.002 ± 0.002 p = 0.1892	Function impaired p < 0.0001
p.Ala387Val (c.1160C>T)	HCO ₃ ⁻ /Cl ⁻ [nM/sec]	0.046 ± 0.027 (4) p = 0.2327	0.054 ± 0.014 (4) p = 0.3218	0.067 ± 0.032 (4) p = 0.5252	0.082 ± 0.053 (4) p = 0.8158	0.100 ± 0.051 (4) p = 0.7995	0.028 ± 0.011 p = 0.023	Function impaired p < 0.0001
	I ⁻ /Cl ⁻ [mM/sec]	0.008 ± 0.005 (3) p = 0.1662	0.016 ± 0.005 (3) p = 0.4038	0.011 ± 0.002 (3) p = 0.2439	0.017 ± 0.008 (3) p = 0.4111	0.015 ± 0.003 (3) p = 0.3413	0.003 ± 0.002 p = 0.1819	Function impaired p < 0.0001
p.Gly389Arg (c.1165G>A)	HCO ₃ ⁻ /Cl ⁻ [nM/sec]	0.054 ± 0.049 (3) p = 0.3825	0.064 ± 0.023 (3) p = 0.5245	0.064 ± 0.015 (3) p = 0.5265	0.071 ± 0.013 (3) p = 0.6367	0.075 ± 0.023 (3) p = 0.6956	0.010 ± 0.009 p = 0.3057	Function impaired p < 0.0001
	I ⁻ /Cl ⁻ [mM/sec]	0.011 ± 0.007 (3) p = 0.2336	0.009 ± 0.005 (3) p = 0.1889	0.012 ± 0.006 (3) p = 0.2642	0.011 ± 0.001 (3) p = 0.2429	0.013 ± 0.004 (3) p = 0.2878	0.001 ± 0.002 p = 0.4214	Function impaired p < 0.0001
p.Gly389Arg (c.1165G>C)	HCO ₃ ⁻ /Cl ⁻ [nM/sec]	0.057 ± 0.015 (3) p = 0.4957	0.110 ± 0.090 (3) p = 0.6993	0.076 ± 0.019 (3) p = 0.7679	0.077 ± 0.012 (3) p = 0.7755	0.113 ± 0.066 (3) p = 0.6584	0.015 ± 0.018 p = 0.408	Function impaired p < 0.0001
	I ⁻ /Cl ⁻ [mM/sec]	0.018 ± 0.008 (3) p = 0.4607	0.014 ± 0.009 (3) p = 0.3203	0.013 ± 0.002 (3) p = 0.3036	0.015 ± 0.002 (3) p = 0.375	0.013 ± 0.002 (3) p = 0.2997	slope < 0 p = 0.4403	Function impaired p < 0.0001
p.Ser391Asn (c.1172G>A)	HCO ₃ ⁻ /Cl ⁻ [nM/sec]	0.076 ± 0.026 (4) p = 0.6844	0.084 ± 0.043 (4) p = 0.8509	0.075 ± 0.024 (4) p = 0.652	0.085 ± 0.048 (4) p = 0.879	0.066 ± 0.022 (4) p = 0.4908	slope < 0 p = 0.6983	Function impaired p < 0.0001
	I ⁻ /Cl ⁻ [mM/sec]	0.012 ± 0.004 (3) p = 0.2746	0.015 ± 0.005 (3) p = 0.3545	0.018 ± 0.001 (3) p = 0.462	0.019 ± 0.007 (3) p = 0.4873	0.024 ± 0.006 (3) p = 0.7334	0.005 ± 0.002 p = 0.0053	Function impaired p < 0.0001
p.Ser391Arg (c.1173C>A)	HCO ₃ ⁻ /Cl ⁻ [nM/sec]	0.049 ± 0.009 (3) p = 0.3588	0.038 ± 0.015 (3) p = 0.2441	0.036 ± 0.039 (3) p = 0.2289	0.056 ± 0.022 (3) p = 0.4346	0.106 ± 0.074 (3) p = 0.7391	0.026 ± 0.014 p = 0.0897	Function impaired p < 0.0001
	I ⁻ /Cl ⁻ [mM/sec]	0.014 ± 0.002 (3) p = 0.2964	0.014 ± 0.003 (3) p = 0.3102	0.015 ± 0.001 (3) p = 0.3437	0.013 ± 0.002 (3) p = 0.2906	0.013 ± 0.001 (3) p = 0.2652	slope < 0 p = 0.4322	Function impaired p < 0.0001
p.Asn392Ser (c.1175A>G)	HCO ₃ ⁻ /Cl ⁻ [nM/sec]	0.049 ± 0.018 (3) p = 0.3348	0.052 ± 0.046 (3) p = 0.3763	0.089 ± 0.041 (3) p = 0.9589	0.056 ± 0.032 (3) p = 0.4347	0.096 ± 0.027 (3) p = 0.9091	0.020 ± 0.012 p = 0.1275	Function impaired p < 0.0001
	I ⁻ /Cl ⁻ [mM/sec]	0.009 ± 0.001 (3) p = 0.1892	0.016 ± 0.003 (3) p = 0.3664	0.015 ± 0.002 (3) p = 0.3464	0.015 ± 0.001 (3) p = 0.340	0.023 ± 0.005 (3) p = 0.6698	0.005 ± 0.001 p = 0.0012	Function impaired p < 0.0001
p.Gly396Glu (c.1187G>A)	HCO ₃ ⁻ /Cl ⁻ [nM/sec]	0.089 ± 0.038 (4) p = 0.9512	0.096 ± 0.060 (4) p = 0.9048	0.121 ± 0.054 (4) p = 0.4323	0.084 ± 0.031 (4) p = 0.852	0.108 ± 0.013 (4) p = 0.6605	0.006 ± 0.013 p = 0.6755	Function impaired p < 0.0001
	I ⁻ /Cl ⁻ [mM/sec]	0.009 ± 0.005 (3) p = 0.1751	0.009 ± 0.001 (3) p = 0.1868	0.012 ± 0.002 (3) p = 0.2536	0.011 ± 0.003 (3) p = 0.2304	0.010 ± 0.002 (3) p = 0.2133	0.001 ± 0.001 p = 0.3095	Function impaired p < 0.0001
p.Val402Met (c.1204G>A)	HCO ₃ ⁻ /Cl ⁻ [nM/sec]	0.086 ± 0.026 (3) p = 0.9029	0.075 ± 0.010 (3) p = 0.7134	0.072 ± 0.029 (3) p = 0.6663	0.108 ± 0.071 (3) p = 0.6978	0.095 ± 0.020 (3) p = 0.9317	0.010 ± 0.013 p = 0.4368	Function impaired p < 0.0001
	I ⁻ /Cl ⁻ [mM/sec]	0.013 ± 0.001 (3) p = 0.2741	0.011 ± 0.003 (3) p = 0.2302	0.016 ± 0.007 (3) p = 0.3718	0.018 ± 0.004 (3) p = 0.4644	0.018 ± 0.003 (3) p = 0.4446	0.004 ± 0.001 p = 0.0321	Function impaired p < 0.0001
p.Thr404Ile (c.1211C>T)	HCO ₃ ⁻ /Cl ⁻ [nM/sec]	0.091 ± 0.032 (5) p = 0.9989	0.062 ± 0.059 (5) p = 0.4374	0.085 ± 0.043 (5) p = 0.870	0.094 ± 0.059 (5) p = 0.940	0.100 ± 0.047 (5) p = 0.8092	0.010 ± 0.013 p = 0.4618	Function impaired p < 0.0001
	I ⁻ /Cl ⁻ [mM/sec]	0.011 ± 0.004 (3) p = 0.2324	0.011 ± 0.004 (3) p = 0.2375	0.014 ± 0.004 (3) p = 0.3348	0.015 ± 0.003 (3) p = 0.365	0.012 ± 0.007 (3) p = 0.2664	0.001 ± 0.002 p = 0.4046	Function impaired p < 0.0001
p.Ala406Thr (c.1216G>A)	HCO ₃ ⁻ /Cl ⁻ [nM/sec]	0.233 ± 0.068 (3) p = 0.0172	0.345 ± 0.073 (3) p = 0.0002	0.473 ± 0.053 (3) p < 0.0001	0.479 ± 0.026 (3) p < 0.0001	0.461 ± 0.088 (3) p < 0.0001	0.118 ± 0.028 p = 0.0011	Function impaired p < 0.0001
	I ⁻ /Cl ⁻ [mM/sec]	0.056 ± 0.009 (3) p = 0.3394	0.094 ± 0.021 (3) p = 0.0308	0.120 ± 0.037 (3) p = 0.005	0.111 ± 0.040 (3) p = 0.0095	0.122 ± 0.033 (3) p = 0.0046	0.030 ± 0.011 p = 0.017	Function impaired p = 0.0212
p.Ser408Asp (c.1222_3TC>CA) *	HCO ₃ ⁻ /Cl ⁻ [nM/sec]	0.040 ± 0.019 (4) p = 0.1339	0.057 ± 0.020 (4) p = 0.3078	0.053 ± 0.012 (4) p = 0.2554	0.070 ± 0.031 (4) p = 0.5357	0.088 ± 0.031 (4) p = 0.919	0.022 ± 0.007 p = 0.0068	Function impaired p < 0.0001
	I ⁻ /Cl ⁻ [mM/sec]	0.011 ± 0.002 (3) p = 0.2394	0.013 ± 0.003 (3) p = 0.276	0.017 ± 0.004 (3) p = 0.4036	0.016 ± 0.007 (3) p = 0.3921	0.019 ± 0.002 (3) p = 0.4893	0.004 ± 0.001 p = 0.0165	Function impaired p < 0.0001
p.Ser408Glu (c.1222_4TCC>GAG) *	HCO ₃ ⁻ /Cl ⁻ [nM/sec]	0.066 ± 0.032 (5) p = 0.477	0.075 ± 0.021 (5) p = 0.6504	0.063 ± 0.034 (5) p = 0.427	0.084 ± 0.059 (5) p = 0.8493	0.091 ± 0.057 (5) p = 0.9929	0.012 ± 0.012 p = 0.3294	Function impaired p < 0.0001
	I ⁻ /Cl ⁻ [mM/sec]	0.008 ± 0.003 (3) p = 0.1561	0.009 ± 0.005 (3) p = 0.1915	0.010 ± 0.002 (3) p = 0.2025	0.015 ± 0.001 (3) p = 0.3308	0.010 ± 0.001 (3) p = 0.2164	0.002 ± 0.001 p = 0.0695	Function impaired p < 0.0001

Figure 2

Table 1. Cont.

		Transport Activity [Mean ± SD (n)]					Dox-Dependence	
		Dox: 0.1 µg/mL	Dox: 0.3 µg/mL	Dox: 1 µg/mL	Dox: 3 µg/mL	Dox: 10 µg/mL	Transport Activity/ log ₁₀ [Dox] (Slope ± SE)	Comparison to WT (F-Test)
p.Arg409Cys (c.1225C>T)	HCO ₃ ⁻ /Cl ⁻ [nM/sec]	0.103 ± 0.066 (3) <i>p</i> = 0.8259	0.091 ± 0.081 (3) <i>p</i> = 0.9943	0.065 ± 0.036 (3) <i>p</i> = 0.6379	0.076 ± 0.040 (3) <i>p</i> = 0.782	0.168 ± 0.085 (3) <i>p</i> = 0.1685	0.023 ± 0.024 <i>p</i> = 0.3529	Function impaired <i>p</i> < 0.0001
	Γ ⁻ /Cl ⁻ [mM/sec]	0.022 ± 0.002 (3) <i>p</i> = 0.6456	0.024 ± 0.002 (3) <i>p</i> = 0.7489	0.028 ± 0.003 (3) <i>p</i> = 0.9292	0.028 ± 0.004 (3) <i>p</i> = 0.9227	0.026 ± 0.004 (3) <i>p</i> = 0.8445	0.002 ± 0.001 <i>p</i> = 0.0791	Function impaired <i>p</i> < 0.0001
p.Arg409Leu (c.1226G>T)	HCO ₃ ⁻ /Cl ⁻ [nM/sec]	0.234 ± 0.042 (4) <i>p</i> = 0.225	0.275 ± 0.037 (4) <i>p</i> = 0.1221	0.318 ± 0.043 (4) <i>p</i> = 0.0603	0.334 ± 0.082 (4) <i>p</i> = 0.0453	0.380 ± 0.044 (3) <i>p</i> = 0.0003	0.071 ± 0.016 <i>p</i> = 0.0004	Function impaired <i>p</i> < 0.0001
	Γ ⁻ /Cl ⁻ [mM/sec]	0.061 ± 0.002 (3) <i>p</i> = 0.0552	0.078 ± 0.005 (3) <i>p</i> = 0.0072	0.086 ± 0.003 (3) <i>p</i> = 0.0027	0.086 ± 0.005 (3) <i>p</i> = 0.0024	0.095 ± 0.013 (3) <i>p</i> = 0.009	0.015 ± 0.003 <i>p</i> < 0.0001	Function impaired <i>p</i> < 0.0001
p.Ala411Pro (c.1231G>C)	HCO ₃ ⁻ /Cl ⁻ [nM/sec]	0.064 ± 0.021 (3) <i>p</i> = 0.5137	0.084 ± 0.021 (3) <i>p</i> = 0.8711	0.071 ± 0.033 (3) <i>p</i> = 0.6193	0.066 ± 0.013 (3) <i>p</i> = 0.5427	0.065 ± 0.014 (3) <i>p</i> = 0.529	slope < 0 <i>p</i> = 0.6639	Function impaired <i>p</i> < 0.0001
	Γ ⁻ /Cl ⁻ [mM/sec]	0.016 ± 0.002 (3) <i>p</i> = 0.3929	0.024 ± 0.002 (3) <i>p</i> = 0.7402	0.027 ± 0.005 (3) <i>p</i> = 0.8987	0.028 ± 0.005 (3) <i>p</i> = 0.9163	0.029 ± 0.005 (3) <i>p</i> = 0.9784	0.006 ± 0.002 <i>p</i> = 0.0033	Function impaired <i>p</i> < 0.0001
p.Ala411Thr (c.1231G>A)	HCO ₃ ⁻ /Cl ⁻ [nM/sec]	0.890 ± 0.010 (3) <i>p</i> < 0.0001	1.176 ± 0.035 (3) <i>p</i> < 0.0001	1.370 ± 0.120 (3) <i>p</i> < 0.0001	1.732 ± 0.237 (3) <i>p</i> < 0.0001	1.752 ± 0.047 (3) <i>p</i> < 0.0001	0.455 ± 0.049 <i>p</i> < 0.0001	WT-like <i>p</i> = 0.0847
	Γ ⁻ /Cl ⁻ [mM/sec]	0.064 ± 0.012 (3) <i>p</i> = 0.0955	0.079 ± 0.014 (3) <i>p</i> = 0.0224	0.094 ± 0.011 (3) <i>p</i> = 0.0054	0.113 ± 0.023 (3) <i>p</i> = 0.0009	0.123 ± 0.022 (3) <i>p</i> = 0.0004	0.030 ± 0.006 <i>p</i> = 0.0001	Function impaired <i>p</i> < 0.0062
p.Val412Ile (c.1234G>A)	HCO ₃ ⁻ /Cl ⁻ [nM/sec]	0.868 ± 0.186 (3) <i>p</i> = 0.041	1.132 ± 0.503 (3) <i>p</i> = 0.0091	1.430 ± 0.706 (3) <i>p</i> = 0.0016	1.530 ± 0.532 (3) <i>p</i> = 0.0009	2.081 ± 0.849 (3) <i>p</i> < 0.0001	0.566 ± 0.194 <i>p</i> = 0.0121	WT-like <i>p</i> = 0.8432
	Γ ⁻ /Cl ⁻ [mM/sec]	0.085 ± 0.009 (3) <i>p</i> = 0.005	0.117 ± 0.005 (3) <i>p</i> = 0.0002	0.122 ± 0.016 (3) <i>p</i> = 0.0001	0.141 ± 0.015 (3) <i>p</i> < 0.0001	0.146 ± 0.006 (3) <i>p</i> < 0.0001	0.029 ± 0.004 <i>p</i> < 0.0001	Function impaired <i>p</i> = 0.0036
p.Gln413Pro (c.1238A>C)	HCO ₃ ⁻ /Cl ⁻ [nM/sec]	0.095 ± 0.021 (3) <i>p</i> = 0.9349	0.081 ± 0.027 (3) <i>p</i> = 0.8519	0.090 ± 0.057 (3) <i>p</i> = 0.984	0.144 ± 0.056 (3) <i>p</i> = 0.3123	0.121 ± 0.100 (3) <i>p</i> = 0.5596	0.023 ± 0.020 <i>p</i> = 0.2745	Function impaired <i>p</i> < 0.0001
	Γ ⁻ /Cl ⁻ [mM/sec]	0.019 ± 0.003 (3) <i>p</i> = 0.4857	0.026 ± 0.007 (3) <i>p</i> = 0.8454	0.027 ± 0.002 (3) <i>p</i> = 0.8783	0.024 ± 0.001 (3) <i>p</i> = 0.7352	0.022 ± 0.004 (3) <i>p</i> = 0.6318	0.001 ± 0.002 <i>p</i> = 0.6167	Function impaired <i>p</i> < 0.0001
p.Gln413Arg (c.1238A>G)	HCO ₃ ⁻ /Cl ⁻ [nM/sec]	0.313 ± 0.107 (3) <i>p</i> = 0.0652	0.349 ± 0.156 (3) <i>p</i> = 0.0349	0.440 ± 0.212 (3) <i>p</i> = 0.0069	0.459 ± 0.203 (3) <i>p</i> = 0.0048	0.424 ± 0.208 (3) <i>p</i> = 0.0092	0.066 ± 0.059 <i>p</i> = 0.2848	Function impaired <i>p</i> < 0.0001
	Γ ⁻ /Cl ⁻ [mM/sec]	0.039 ± 0.011 (3) <i>p</i> = 0.5267	0.050 ± 0.009 (3) <i>p</i> = 0.1857	0.058 ± 0.002 (3) <i>p</i> = 0.0756	0.064 ± 0.002 (3) <i>p</i> = 0.0391	0.072 ± 0.007 (3) <i>p</i> = 0.0139	0.016 ± 0.002 <i>p</i> < 0.0001	Function impaired <i>p</i> = 0.0001
p.Glu414Lys (c.1240G>A)	HCO ₃ ⁻ /Cl ⁻ [nM/sec]	0.305 ± 0.075 (3) <i>p</i> = 0.0431	0.314 ± 0.166 (3) <i>p</i> = 0.0356	0.327 ± 0.079 (3) <i>p</i> = 0.0279	0.404 ± 0.106 (3) <i>p</i> = 0.0055	0.429 ± 0.262 (3) <i>p</i> = 0.0033	0.067 ± 0.050 <i>p</i> = 0.1998	Function impaired <i>p</i> < 0.0001
	Γ ⁻ /Cl ⁻ [mM/sec]	0.040 ± 0.008 (3) <i>p</i> = 0.4681	0.045 ± 0.007 (3) <i>p</i> = 0.3109	0.049 ± 0.002 (3) <i>p</i> = 0.2121	0.051 ± 0.005 (3) <i>p</i> = 0.1617	0.061 ± 0.008 (3) <i>p</i> = 0.0545	0.010 ± 0.002 <i>p</i> = 0.0007	Function impaired <i>p</i> < 0.0001
p.Ser415Gly (c.1243A>G)	HCO ₃ ⁻ /Cl ⁻ [nM/sec]	0.384 ± 0.171 (3) <i>p</i> = 0.0303	0.484 ± 0.075 (3) <i>p</i> = 0.0059	0.727 ± 0.184 (3) <i>p</i> = 0.0001	0.824 ± 0.260 (3) <i>p</i> < 0.0001	0.774 ± 0.260 (3) <i>p</i> < 0.0001	0.224 ± 0.070 <i>p</i> = 0.0072	Function impaired <i>p</i> < 0.0001
	Γ ⁻ /Cl ⁻ [mM/sec]	0.068 ± 0.011 (3) <i>p</i> = 0.0377	0.089 ± 0.011 (3) <i>p</i> = 0.0039	0.097 ± 0.014 (3) <i>p</i> = 0.0017	0.107 ± 0.016 (3) <i>p</i> = 0.0006	0.112 ± 0.007 (3) <i>p</i> = 0.0003	0.021 ± 0.004 <i>p</i> = 0.0002	Function impaired <i>p</i> = 0.0007
p.Ser415Arg (c.1245C>A)	HCO ₃ ⁻ /Cl ⁻ [nM/sec]	0.634 ± 0.135 (3) <i>p</i> < 0.0001	0.923 ± 0.072 (3) <i>p</i> < 0.0001	0.915 ± 0.013 (3) <i>p</i> < 0.0001	1.084 ± 0.041 (3) <i>p</i> < 0.0001	1.242 ± 0.057 (3) <i>p</i> < 0.0001	0.275 ± 0.033 <i>p</i> < 0.0001	Function impaired <i>p</i> < 0.0001
	Γ ⁻ /Cl ⁻ [mM/sec]	0.052 ± 0.009 (3) <i>p</i> = 0.203	0.069 ± 0.018 (3) <i>p</i> = 0.0371	0.080 ± 0.011 (3) <i>p</i> = 0.0102	0.094 ± 0.010 (3) <i>p</i> = 0.0023	0.091 ± 0.013 (3) <i>p</i> = 0.0033	0.021 ± 0.004 <i>p</i> = 0.0005	Function impaired <i>p</i> = 0.0006
p.Ser532Ile (c.1595G>T)	HCO ₃ ⁻ /Cl ⁻ [nM/sec]	0.549 ± 0.091 (4) <i>p</i> = 0.0011	0.793 ± 0.254 (4) <i>p</i> < 0.0001	0.816 ± 0.107 (4) <i>p</i> < 0.0001	0.845 ± 0.267 (4) <i>p</i> < 0.0001	0.912 ± 0.245 (4) <i>p</i> < 0.0001	0.155 ± 0.063 <i>p</i> = 0.0244	Function impaired <i>p</i> < 0.0001
	Γ ⁻ /Cl ⁻ [mM/sec]	0.053 ± 0.011 (3) <i>p</i> = 0.2373	0.055 ± 0.011 (3) <i>p</i> = 0.198	0.069 ± 0.018 (3) <i>p</i> = 0.0572	0.086 ± 0.028 (3) <i>p</i> = 0.0108	0.095 ± 0.009 (3) <i>p</i> = 0.0045	0.023 ± 0.006 <i>p</i> = 0.0011	Function impaired <i>p</i> = 0.0015
p.Ala104Val (c.311C>T)	HCO ₃ ⁻ /Cl ⁻ [nM/sec]	0.079 ± 0.017 (4) <i>p</i> = 0.7598	0.152 ± 0.080 (4) <i>p</i> = 0.1325	0.110 ± 0.035 (4) <i>p</i> = 0.6295	0.132 ± 0.029 (4) <i>p</i> = 0.3075	0.105 ± 0.039 (4) <i>p</i> = 0.718	0.006 ± 0.015 <i>p</i> = 0.7015	Function impaired <i>p</i> < 0.0001
	Γ ⁻ /Cl ⁻ [mM/sec]	0.363 ± 0.051 (6) <i>p</i> < 0.0001	0.402 ± 0.075 (6) <i>p</i> < 0.0001	0.468 ± 0.039 (6) <i>p</i> < 0.0001	0.528 ± 0.100 (6) <i>p</i> < 0.0001	0.443 ± 0.084 (6) <i>p</i> < 0.0001	0.057 ± 0.022 <i>p</i> = 0.0159	Function impaired <i>p</i> < 0.0001
p.Ala451Gly (c.1352C>G) *	HCO ₃ ⁻ /Cl ⁻ [nM/sec]	0.479 ± 0.092 (3) <i>p</i> = 0.0062	0.911 ± 0.063 (3) <i>p</i> < 0.0001	0.993 ± 0.129 (3) <i>p</i> < 0.0001	1.284 ± 0.089 (3) <i>p</i> < 0.0001	1.836 ± 0.184 (3) <i>p</i> < 0.0001	0.618 ± 0.056 <i>p</i> = 0.0001	WT-like <i>p</i> = 0.7423
	Γ ⁻ /Cl ⁻ [mM/sec]	0.572 ± 0.140 (3) <i>p</i> = 0.0027	0.921 ± 0.162 (3) <i>p</i> < 0.0001	1.168 ± 0.127 (3) <i>p</i> < 0.0001	1.406 ± 0.167 (3) <i>p</i> < 0.0001	1.749 ± 0.251 (3) <i>p</i> < 0.0001	0.568 ± 0.057 <i>p</i> = 0.0001	WT-like <i>p</i> = 0.7667
p.Ala451Leu (c.1351_2GC>CT) *	HCO ₃ ⁻ /Cl ⁻ [nM/sec]	0.097 ± 0.047 (3) <i>p</i> = 0.3455	0.144 ± 0.013 (3) <i>p</i> = 0.0283	0.100 ± 0.036 (3) <i>p</i> = 0.3058	0.093 ± 0.014 (3) <i>p</i> = 0.4034	0.143 ± 0.064 (3) <i>p</i> = 0.0299	0.008 ± 0.015 <i>p</i> = 0.6021	Function impaired <i>p</i> < 0.0001

Bold fonts were used to emphasize the amino acid changes of the variants from nucleotide changes in the parentheses.

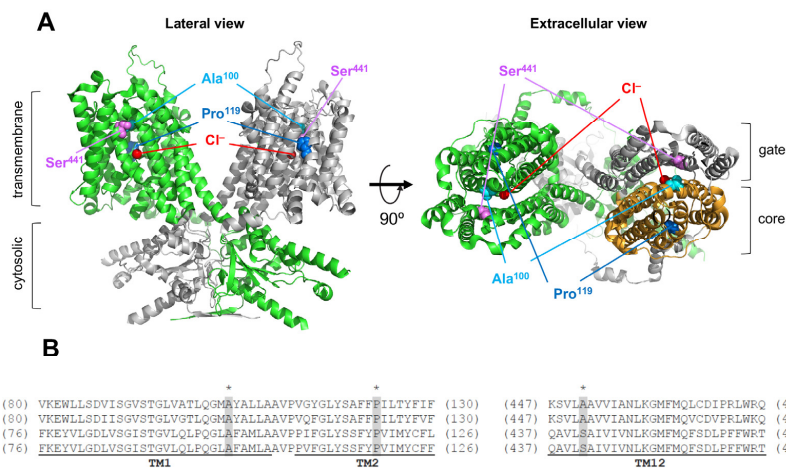


Figure 3. Ala¹⁰⁰, Pro¹¹⁹, and Ser⁴⁴¹ sites in prestin. **(A)** The homodimeric structure of human prestin (PDB: 7LGU). Protomers are shown in green and gray. In right panel, the core domain of one of the protomers is shown in bright orange. The Ala¹⁰⁰, Pro¹¹⁹, and Ser⁴⁴¹ sites and bound chlorides are indicated by cyan, blue, purple, and red spheres, respectively. **(B)** Partial amino acid sequences of human and mouse pendrin (A4) and prestin (A5). Numbers in parentheses indicate the residue numbers at the N- and C-terminal ends. The residues with asterisks indicate Ala¹⁰⁰, Pro¹¹⁹, and Ser⁴⁴¹ in human prestin (hA5) and equivalents in others.

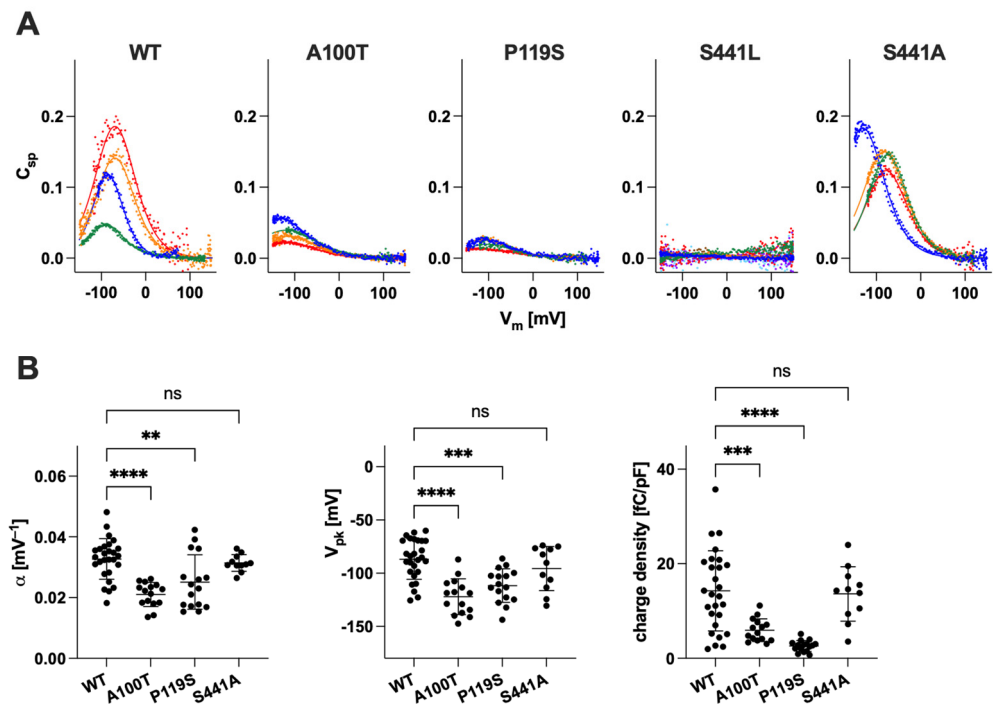


Figure 4. NLC measurements. (A) Examples of NLC recorded in HEK293T cells expressing WT, p.A100T, p.P119S, p.S441L, or p.S441A prestin. Different colors indicate individual recordings. (B) Summaries of the NLC parameters (α , V_{pk} , and CD). Error bars indicate SD. ns, $p \geq 0.05$; ** $0.001 < p \leq 0.01$; *** $0.0001 < p \leq 0.001$; **** $p \leq 0.0001$.

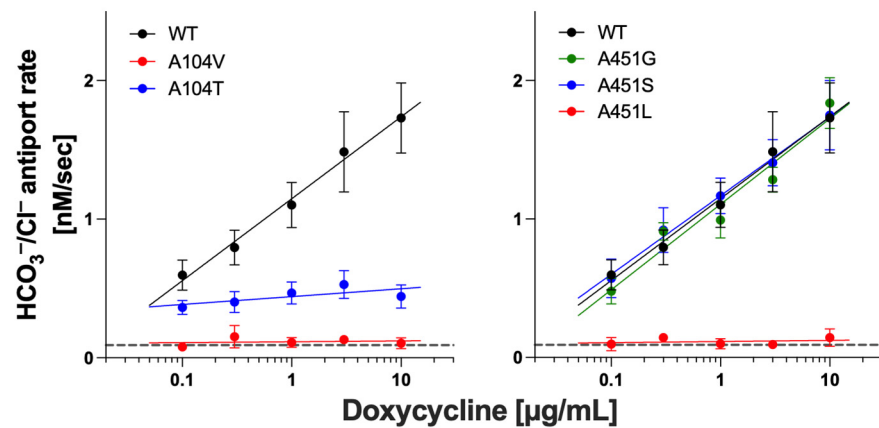


Figure 5. The effects of missense changes at Ala¹⁰⁴ and Ala⁴⁵¹ on the anion transport function of pendrin. HCO_3^-/Cl^- antiport assay conducted for p.A104V (left), p.A104T (left), p.A451G (right), p.A451S (right), and p.A451L (right) pendrin alongside WT control. Error bars indicate SD. Horizontal dotted lines indicate transport rates of uninduced cells. Solid lines indicate linear regressions (\log_{10} [Dox] vs. transport rates). Sample size information and statistics are provided in Table 1.

2.3. Comparison to AlphaMissense Variant Effect Predictor

The pathogenicity of disease-associated variants is best assessed by functional analyses such as those presented here; however, experimental characterization of variants is laborious and remains reactive to the rapid identification of novel variants. Recent advancements in computational methods using machine learning have prompted us to evaluate the performance of AlphaMissense (AM), a novel tool for predicting the pathogenicity of missense variants [16]. First, we visualized the provided AM prediction scores of pendrin and prestin at every amino acid position as heatmaps (Supplementary Figures S1 and S2).

AM pathogenicity predictions for both pendrin and prestin show similarity, such as (i) variants in regions that lack structural information (C- and N-termini, IDR) tend to be benign (i.e., predominantly “blue”); and (ii) variants in transmembrane regions tend to be less tolerant to missense changes (i.e., predominantly “red”) in the heatmap (Supplementary Figures S1 and S2). These observations are in line with the fact that AM utilizes structural information, and both pendrin and prestin share quite similar overall molecular architecture. To evaluate the accuracy of AM, we plotted the $\text{HCO}_3^-/\text{Cl}^-$ antiporter activities of pendrin variants measured in our previous study [10] and this study, which are normalized to WT control, against the AM pathogenicity scores (Figure 6). We found an overall correlation between our functional assay data and AM prediction scores of $r = -0.6497$ (nonparametric Spearman correlation), which is in line with the example given in their report (GCK, $r = -0.65$, Figure 3G in [16]). Many variants tested in this study are clustered around highly conserved TM9-10 that are essential for the transport function, and thus many had little or no activities, skewing the distribution of variants (Figure 6, inset). In addition, we found several variants that were misclassified by AM as benign when there is vastly reduced activity (for example, p.N392S) or vice versa (ambiguous/pathogenic when their activity is WT-like, such as p.T307A, p.L117F, and p.F354S) (Table 2). For prestin variants, AM scores for p.A100T, p.P119S, and p.S441L were 0.9138, 0.7712, and 0.916, respectively, all predicted to be pathogenic.

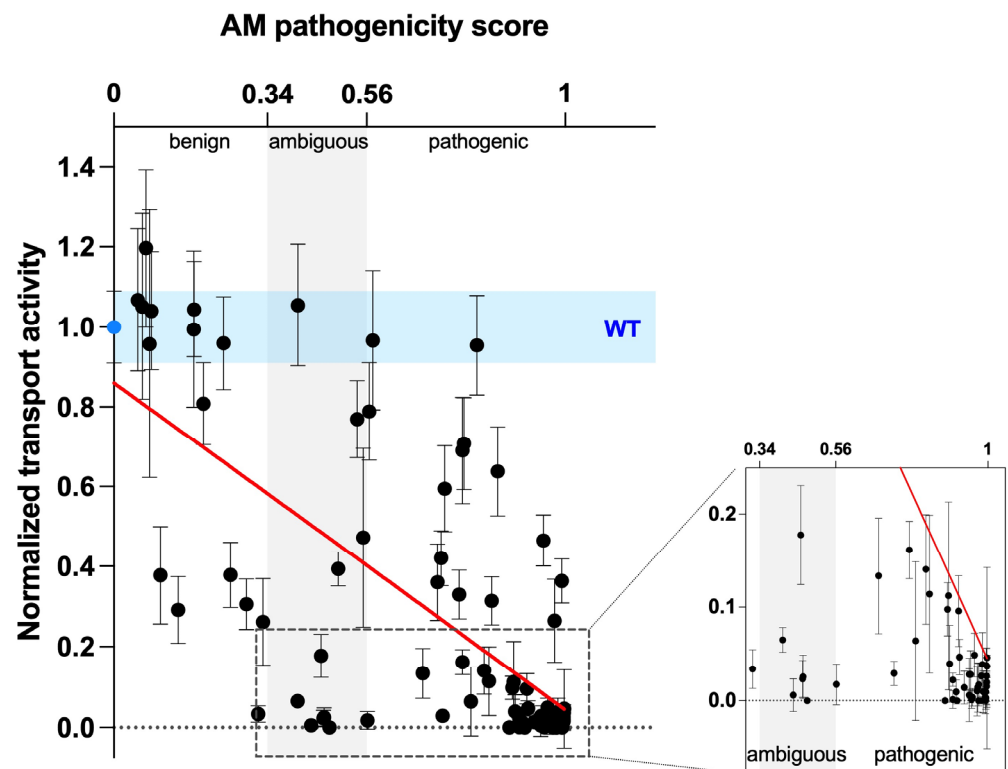


Figure 6. Correlation with AlphaMissense pathogenicity scores. $\text{HCO}_3^-/\text{Cl}^-$ transport rates of pendrin WT and variants from this study and the previous study [10] were normalized to the WT value and plotted against AlphaMissense (AM) pathogenicity scores [16]. Light blue shades indicate $\text{HCO}_3^-/\text{Cl}^-$ rate of WT with errors (propagated errors). Gray shade between AM scores 0.34–0.56 marks the “ambiguous” category, with scores lower being “benign” and higher being “pathogenic” as indicated. Red line indicates the linear fit between the $\text{HCO}_3^-/\text{Cl}^-$ antiporter activity and the AM scores. Inset: Region indicated by the broken lines in left are enlarged to visualize variants with little or no $\text{HCO}_3^-/\text{Cl}^-$ transport activity.

Table 2. Comparison of experimental data vs. AM scores. The slope values of the Dox-dependent HCO₃⁻ /Cl⁻ antiport activities from our previous study [10] and from this study for each variant were normalized to WT. For variants with negative slope values (slope < 0), normalized activity of 0 was assigned (highlighted in yellow) with no error propagations. Variants with WT-like HCO₃⁻ /Cl⁻ antiport activity (p ≥ 0.05) were shaded in light blue, and ones with impaired functions (p < 0.05) are shaded in pale pink. AM scores for pathogenicity classification uses the same color shades as in Supplementary Figures S1 and S2. Asterisks (*) indicate variants not found in human patients (as of January 2024).

	HCO ₃ ⁻ /Cl ⁻ Antiport Assay Results		AM Prediction	
	%WT Activity	Variant Effect	AM Score	AM Category
p.Ser28Gly (c.82A>G)	29.2 ± 8.3	Function impaired	0.1421	benign
p.Ser49Arg (c.147C>G)	104.1 ± 13.7	WT-like	0.0831	benign
p.Pro76Ser (c.226C>T)	30.5 ± 6.3	Function impaired	0.2937	benign
p.Ser90Leu (c.269C>T)	0.1 ± 0.9	Function impaired	0.8985	pathogenic
p.Thr99Arg (c.296C>G)	0	Function impaired	0.9802	pathogenic
p.Leu117Phe (c.349C>T)	95.5 ± 12.5	WT-like	0.804	pathogenic
p.Pro123Ser (c.367C>T)	2.9 ± 1.3	Function impaired	0.7286	pathogenic
p.Gly131Val (c.392G>T)	0.4 ± 1.7	Function impaired	0.9925	pathogenic
p.Ser133Thr (c.397T>A)	2.3 ± 2.0	Function impaired	0.4642	ambiguous
p.Gly139Ala (c.416G>C)	0	Function impaired	0.9105	pathogenic
p.Met147Thr (c.440T>C)	0.6 ± 2.8	Function impaired	0.9459	pathogenic
p.Met147Val (c.439A>G)	6.4 ± 8.5	Function impaired	0.7909	pathogenic
p.Val163Ile (c.487G>A)	105.1 ± 23.2	WT-like	0.0632	benign
p.Val186Phe (c.556G>T)	0	Function impaired	0.4777	ambiguous
p.Thr193Ile (c.578C>T)	0.9 ± 1.3	Function impaired	0.9082	pathogenic
p.Tyr214Cys (c.641A>G)	31.4 ± 6.0	Function impaired	0.8371	pathogenic
p.Val239Asp (c.716T>A)	4.9 ± 2.3	Function impaired	0.9612	pathogenic
p.Asp266Asn (c.796G>A)	106.7 ± 17.7	WT-like	0.0528	ambiguous
p.Thr307Ala (c.919A>G)	105.5 ± 15.2	WT-like	0.4074	ambiguous
p.Asn324Tyr (c.970A>T)	99.4 ± 19.5	WT-like	0.1773	pathogenic
p.Gly334Val (c.1001G>T)	59.5 ± 10.8	Function impaired	0.7329	pathogenic
p.Phe354Ser (c.1061T>C)	96.6 ± 17.4	WT-like	0.5739	pathogenic
p.Lys369Glu (c.1105A>G)	39.4 ± 4.2	Function impaired	0.4968	ambiguous
p.Ala372Val (c.1115C>T)	0.1 ± 0.9	Function impaired	0.9528	pathogenic
p.Asn392Tyr (c.1174A>T)	0.5 ± 0.7	Function impaired	0.9493	pathogenic
p.Ser399Pro (c.1195T>C)	78.9 ± 12.2	Function impaired	0.5658	pathogenic
p.Ser408Phe (c.1223C>T)	0.9 ± 1.3	Function impaired	0.9938	pathogenic
p.Arg409His (c.1226G>A)	2.8 ± 2.6	Function impaired	0.9499	pathogenic
p.Thr410Lys (c.1229C>A)	1.9 ± 1.1	Function impaired	0.9957	pathogenic
p.Thr410Met (c.1229C>T)	1.4 ± 1.7	Function impaired	0.9314	pathogenic
p.Thr416Pro (c.1246A>C)	2.2 ± 0.7	Function impaired	0.8985	pathogenic
p.Gln421Leu (c.1262A>T)	14.1 ± 5.9	Function impaired	0.8205	pathogenic
p.Ile426Asn (c.1277T>A)	63.8 ± 11.2	Function impaired	0.8501	pathogenic
p.Leu445Irp (c.1334T>G)	0	Function impaired	0.9933	pathogenic
p.Asn457Lys (c.1371C>A)	36.4 ± 5.5	Function impaired	0.992	pathogenic
p.Arg470His (c.1409G>A)	119.6 ± 19.7	WT-like	0.0709	benign
p.Val483Glu (c.1448T>A)	70.7 ± 11.6	WT-like	0.7757	pathogenic
p.Gly497Ser (c.1489G>A)	9.8 ± 2.9	Function impaired	0.883	pathogenic
p.Thr527Pro (c.1579A>C)	42.0 ± 6.8	Function impaired	0.7253	pathogenic
p.Ile529Ser (c.1586T>G)	16.1 ± 3.1	Function impaired	0.7726	pathogenic
p.Tyr556Cys (c.1667A>G)	6.5 ± 1.3	Function impaired	0.4069	ambiguous
p.Cys565Tyr (c.1694G>A)	80.8 ± 10.3	WT-like	0.1986	benign
p.Ser657Asn (c.1970G>A)	33.0 ± 6.0	Function impaired	0.7648	pathogenic
p.Val659Leu (c.1975G>C)	37.9 ± 8.1	Function impaired	0.2582	benign
p.Ser666Phe (c.1997C>T)	17.8 ± 5.3	Function impaired	0.4588	ambiguous
p.Asp669Glu (c.2007C>A)	0.0 ± 0.0	Function impaired	0.973	pathogenic
p.Phe683Ser (c.2048T>C)	2.8 ± 1.8	Function impaired	0.9461	pathogenic
p.Phe692Leu (c.2074T>C)	36.0 ± 9.6	Function impaired	0.7169	pathogenic
p.Leu703Pro (c.2108T>C)	0.3 ± 0.9	Function impaired	0.955	pathogenic
p.Thr721Met (c.2162C>T)	0.6 ± 1.7	Function impaired	0.4373	ambiguous
p.His723Arg (c.2168A>G)	13.4 ± 6.2	Function impaired	0.684	pathogenic
p.Gln383Glu (c.1147C>G)	2.5 ± 2.4	Function impaired	0.4658	ambiguous
p.Glu384Gly (c.1151G>C)	2.7 ± 1.4	Function impaired	0.9808	pathogenic
p.Ala387Val (c.1160C>T)	4.7 ± 1.9	Function impaired	0.9179	pathogenic
p.Gly389Arg (c.1165G>A)	1.7 ± 1.5	Function impaired	0.996	pathogenic
p.Gly389Arg (c.1165G>C)	2.5 ± 3.1	Function impaired	0.996	pathogenic
p.Ser391Asn (c.1172G>A)	0	Function impaired	0.8762	pathogenic
p.Ser391Arg (c.1173C>A)	4.3 ± 2.4	Function impaired	0.9974	pathogenic
p.Asn392Ser (c.1175A>G)	3.4 ± 2.0	Function impaired	0.3199	benign
p.Gly396Glu (c.1187G>A)	1.0 ± 0.2	Function impaired	0.9866	pathogenic
p.Val402Met (c.1204G>A)	1.7 ± 2.2	Function impaired	0.5617	pathogenic
p.Thr404Ile (c.1211C>T)	1.7 ± 2.2	Function impaired	0.9734	pathogenic
p.Ala406Thr (c.1216G>A)	20.0 ± 4.9	Function impaired	0.8845	pathogenic

Wasano et al., 2020 [10]

This study

Table 2. Cont.

	HCO ₃ ⁻ /Cl ⁻ Antiport Assay Results		AM Prediction	
	%WT Activity	Variant Effect	AM Score	AM Category
p.Ser408Asp (c.1222_3TC>GA) *	3.7 ± 1.2	Function impaired	0.9971	pathogenic
p.Ser408Glu (c.1222_4TCC>GAG) *	2.0 ± 2.0	Function impaired	0.9964	pathogenic
p.Arg409Cys (c.1225C>T)	3.4 ± 4.1	Function impaired	0.8893	pathogenic
p.Arg409Leu (c.1226G>T)	12.0 ± 2.8	Function impaired	0.9763	pathogenic
p.Ala411Pro (c.1231G>C)	0	Function impaired	0.9893	pathogenic
p.Ala411Thr (c.1231G>A)	77.0 ± 9.8	WT-like	0.5393	ambiguous
p.Val412Ile (c.1234G>A)	95.8 ± 33.5	WT-like	0.0792	benign
p.Gln413Pro (c.1238A>C)	3.9 ± 3.4	Function impaired	0.9839	pathogenic
p.Gln413Arg (c.1238A>G)	11.2 ± 10.0	Function impaired	0.8859	pathogenic
p.Glu414Lys (c.1240G>A)	11.3 ± 8.5	Function impaired	0.8309	pathogenic
p.Ser415Gly (c.1243A>G)	37.9 ± 12.1	Function impaired	0.1027	benign
p.Ser415Arg (c.1245C>A)	46.5 ± 6.4	Function impaired	0.9514	pathogenic
p.Ser532Ile (c.1595G>T)	26.2 ± 10.8	Function impaired	0.3304	benign
p.Ala104Val (c.311C>T)	1.0 ± 2.5	Function impaired	0.9684	pathogenic
p.Ala104Thr (c.310G>A) *	9.6 ± 3.8	Function impaired	0.9153	pathogenic
p.Ala451Gly (c.1352C>G) *	104.6 ± 11.8	WT-like	0.1774	benign
p.Ala451Ser (c.1351G>T) *	96.1 ± 11.6	WT-like	0.2429	benign
p.Ala451Leu (c.1351_2GC>CT) *	1.4 ± 2.5	Function impaired	0.9707	pathogenic

Bold font was used to distinguish between amino acid changes in the variants and the nucleotide change in the parentheses.

3. Discussion

Precisely understanding the relationships between genotypes and disease phenotypes is the holy grail of the field of human genetics. Although sequencing information becomes more and more accessible, assigning pathogenicity to variations of sequences remains challenging due to the complexity of determining the causality of variants to disease states [69]. Although experimental interrogation is ideal, our collective experimental efforts have only scratched the surface of building an atlas of variant effects in the genome. Consequently, the vast majority of disease-associated variants, including those of pendrin and prestin, remain as variants of unknown significance (VUS) [70]. To bridge the gap, in silico tools have been developed to predict whether a variant plays a causative role in a disease state. Large numbers of variant effect predictors (VEPs) have been reported over the years using various approaches with various degrees of performance [71]. For the deafness genes, a measure for protein-folding stability was used to re-classify VUSs in patients due to protein misfolding [72]. Recently developed AlphaMissense (AM) also uses structural information, although it does not predict protein stability. Rather, it classifies missense variants as benign, ambiguous, or pathogenic based on their prediction scores [16]. As the study provided AM prediction across the entire human proteome, we compared the available AM prediction scores for pendrin to our experimental results on quantitated transport activities. We found a good correlation ($r = -0.6497$, Figure 6), demonstrating their utility in informing the variant effects. It must be noted, however, that the uncertainty still exists as several pendrin variants were misclassified. Thus, the usage of VEPs, even the one that demonstrated superior performance over many existing VEPs across multiple benchmarks as AM, must exercise the utmost caution in clinical settings.

Recent efforts in large-scale systemic studies (multiplexed assay of variant effects, MAVE) have reported functional consequences of hundreds of thousands of variants across genome regions to date [73,74]. For proteins such as pendrin and prestin, however, large-scale multiplexing assays will be challenging as their dysfunctions may not result in easily discernible cellular phenotypes. Nevertheless, our small-scale in vitro assays are robust in determining the degrees of functional impairment of the variants found in human patients. The large variation in PDS and DFN4 phenotypes suggests large variations in the activities of pendrin variants, thus warranting an experimental approach that can detect a subtle difference in transport activities. One caveat will be that our approach to heterologous expression systems may not be able to address the effects of variants on protein expression levels in the host environment, as we forcibly induce protein expression by doxycycline from cDNAs for our transporter assays. Also not addressed here are the variant effects on protein-protein interactions. For example, the intrinsically disordered region (IDR)

within the cytosolic domain of prestin mediates the binding of calmodulin, thereby allowing modulation of protein activity by calcium, which is likely conserved in other SLC26 proteins, including pendrin [75]. Additionally, IQ-motif containing GTPase-activating protein 1 (IQGAP1) was shown to interact with the C-terminal region of pendrin and enhance its transport activity in kidney cells [76]. Interestingly, co-expression of IQGAP1 and pendrin also enhanced the plasma membrane (PM) localization of pendrin, suggesting another layer of regulatory interaction. It is curious that although both pendrin and prestin are conserved and the handful of disease-associated variants in prestin also similarly affected pendrin in this study, prestin is targeted to the lateral membrane in the outer hair cells (OHCs), while pendrin is targeted to the apical membranes of epithelial cells in the thyroid and in the inner ear [77–80]. Thus, it will require additional considerations such as co-expression of interacting partners or using the host cell lines in order to interrogate the effects on variants found in regions where such regulatory interactions were reported in the future.

Although functional annotation of deafness-associated variations in the genome may not be complete until the hearing phenotype is assessed *in vivo*, our continuing efforts to characterize missense variants *in vitro* provide invaluable information regarding the variant effects, which can be used to prioritize future efforts at the organismal level. With ever-improving VEPs such as AM, future studies will provide clinically useful information of variant effects with more confidence.

4. Materials and Methods

4.1. Generation of Stable Cell Lines

cDNAs coding human pendrin (NM_000441.2) and gerbil prestin (AF230376.2), (WT and variants) with a mTurquoise (mTq2) tag on the C-terminus were cloned into a pSBtet-pur vector (Addgene, Watertown, NY, USA) using SfiI sites. Stable cell lines carrying these constructs were established in HEK293T cells as previously described [10]. Stable cells were maintained in DMEM supplemented with 10% FBS and 1 $\mu\text{g}/\text{mL}$ puromycin (Thermo Fisher Scientific, Waltham, MA, USA), and the expression of the pendrin and prestin constructs were induced by the addition of doxycycline (Dox) in the media. For I^-/Cl^- antiport assay, the pendrin-expressing pSBtet-Pur vectors were transfected in the HEK293T cell line that constitutively express mVenus^{p.H148Q/p.I152L} as previously described [10].

4.2. Fluorometric Anion Transport Assays

Fluorometric $\text{HCO}_3^-/\text{Cl}^-$ and I^-/Cl^- antiport assays were established and described in detail in a previous study [10]. Briefly, for $\text{HCO}_3^-/\text{Cl}^-$ antiport assay, stable HEK293T cells expressing pendrin constructs were loaded with a pH indicator, SNARF-5F (S23923, Thermo Fisher Scientific, Waltham, MA, USA) in a high chloride buffer containing (mM): 140 NaCl, 4.5 KCl, 1 MgCl_2 , 2.5 CaCl_2 , 20 HEPES (pH 7.4). The antiport assay was initiated by an automated injection of a low chloride buffer containing (mM): 125 Na-gluconate, 5 K-gluconate, 1 MgCl_2 , 1 CaCl_2 , 20 HEPES, 25 NaHCO_3 with 5% CO_2 in Synergy Neo2 (Agilent/BioTek, Santa Clara, CA, USA). The fluorescence of SNARF-5F were measured in a time dependent manner using Synergy Neo2 (Agilent/BioTek) and the data analyzed offline as described previously [10]. For I^-/Cl^- antiport assay, cells expressing both pendrin variants and iodide sensitive fluorescent protein, mVenus^{p.H148Q/p.I152L}, were resuspended in 200 μL of a high Cl^- buffer containing (mM): 150 NaCl, 1 MgCl_2 , 1 CaCl_2 , 20 HEPES, (pH 7.5). The I^-/Cl^- antiport assay using 160 μL of the cell suspension was initiated by an automated injection of 80 μL of a high I^- buffer containing (mM): 150 NaI, 1 MgCl_2 , 1 CaCl_2 , 20 HEPES (pH 7.5) in Synergy Neo2 (Agilent/BioTek). The fluorescence intensities of mVenus^{p.H148Q/p.I152L} and mTq2 were simultaneously measured in a time-dependent manner using Synergy Neo2 (Agilent/BioTek) and the data analyzed offline as described previously [10].

4.3. Whole-Cell Recordings

Whole-cell recordings were performed at room temperature using the Axopatch 200B amplifier (Molecular Devices, San Jose, CA, USA) with a 10 kHz low-pass filter. Recording pipettes pulled from borosilicate glass were filled with an ionic blocking intracellular solution containing (mM): 140 CsCl, 2 MgCl₂, 10 EGTA, and 10 HEPES (pH 7.4). Cells were bathed in an extracellular solution containing (mM): 120 NaCl, 20 TEA-Cl, 2 CoCl₂, 2 MgCl₂, 10 HEPES (pH 7.4). Osmolality was adjusted to 309 mOsmol/kg with glucose. Holding potentials were set to 0 mV. NLC was measured using sinusoidal voltage stimuli (2.5-Hz, 120 or 150 mV amplitude) superimposed with two higher frequency stimuli (390.6 and 781.2 Hz, 10 mV amplitude). Data were collected by jClamp (SciSoft Company, New Haven, CT, USA) [81].

4.4. NLC Data Analysis

Voltage-dependent C_m data were analyzed using the following two-state Boltzmann equation:

$$C_m = \frac{\alpha Q_{max} \exp[\alpha(V_m - V_{pk})]}{\{1 + \exp[\alpha(V_m - V_{pk})]\}^2} + C_{lin} \quad (1)$$

where α is the slope factor of the voltage-dependence of charge transfer, Q_{max} is the maximum charge transfer, V_m is the membrane potential, V_{pk} is the voltage at which the maximum charge movement is attained, and C_{lin} is the linear capacitance. The specific capacitance, C_{sp} , was calculated as $(C_m - C_{lin})/C_{lin}$.

4.5. Statistical Analyses

Statistical analyses for fluorometric antiport assays were performed as previously described [10]. Briefly, five different Dox dosage conditions were compared to the rates of uninduced cells by one-way ANOVA followed by an uncorrected Fisher's Least Significant Difference (LSD). To assess the dependency of the transport rates on Dox dosage, linear regressions (\log_{10} [Dox] vs. transport rates) were performed. F tests were performed to find the difference in the Dox-dependence between WT versus pendrin variants. To obtain normalized activities for each pendrin variant, the slope value from the linear regressions described above was divided by that of WT. The uncertainties (σ) associated with division computations were calculated as previously described [82] using the following equation:

$$\sigma_{A/B} = \left| \frac{A}{B} \right| \sqrt{\left(\frac{\sigma_A}{A}\right)^2 + \left(\frac{\sigma_B}{B}\right)^2} \quad (2)$$

where A and B are the mean values with associated errors in linear regressions, σ_A and σ_B , respectively. These values are reported as errors in Table 2 under "%WT Activity". The Spearman Correlation coefficient (r) between pendrin HCO₃⁻/Cl⁻ transport activities and the AM scores was calculated using Prism 10.2.0. For NLC data analyses, a one-way ANOVA combined with Tukey's post hoc test was used for multiple comparisons. In all statistical tests, $p < 0.05$ was considered statistically significant.

Supplementary Materials: The following supporting information can be downloaded at: <https://www.mdpi.com/article/10.3390/ijms25052759/s1>.

Author Contributions: Conceptualization, K.H.; investigation, S.T., T.K., K.W. and K.H.; formal analysis, S.T. and K.H.; visualization, S.T. and K.H.; writing—original draft preparation, S.T.; writing—review and editing, S.T. and K.H.; funding acquisition, K.H. All authors have read and agreed to the published version of the manuscript.

Funding: This research was funded by NIH grant DC017482 to K. H. and the Hugh Knowles Center.

Institutional Review Board Statement: Not applicable.

Informed Consent Statement: Not applicable.

Data Availability Statement: The original contributions presented in the study are included in the article/Supplementary Materials, further inquiries can be directed to the corresponding author.

Conflicts of Interest: The authors declare no conflicts of interests.

References

1. Choi, B.Y.; Kim, H.M.; Ito, T.; Lee, K.Y.; Li, X.; Monahan, K.; Wen, Y.; Wilson, E.; Kurima, K.; Saunders, T.L.; et al. Mouse model of enlarged vestibular aqueducts defines temporal requirement of Slc26a4 expression for hearing acquisition. *J. Clin. Investig.* **2011**, *121*, 4516–4525. [[CrossRef](#)]
2. Everett, L.A.; Belyantseva, I.A.; Noben-Trauth, K.; Cantos, R.; Chen, A.; Thakkar, S.I.; Hoogstraten-Miller, S.L.; Kachar, B.; Wu, D.K.; Green, E.D. Targeted disruption of mouse Pds provides insight about the inner-ear defects encountered in Pendred syndrome. *Hum. Mol. Genet.* **2001**, *10*, 153–161. [[CrossRef](#)]
3. Zheng, J.; Shen, W.; He, D.Z.; Long, K.B.; Madison, L.D.; Dallos, P. Prestin is the motor protein of cochlear outer hair cells. *Nature* **2000**, *405*, 149–155. [[CrossRef](#)]
4. Liberman, M.C.; Gao, J.; He, D.Z.; Wu, X.; Jia, S.; Zuo, J. Prestin is required for electromotility of the outer hair cell and for the cochlear amplifier. *Nature* **2002**, *419*, 300–304. [[CrossRef](#)]
5. Cheatham, M.A.; Huynh, K.H.; Gao, J.; Zuo, J.; Dallos, P. Cochlear function in Prestin knockout mice. *J. Physiol.* **2004**, *560*, 821–830. [[CrossRef](#)]
6. Dallos, P.; Wu, X.; Cheatham, M.A.; Gao, J.; Zheng, J.; Anderson, C.T.; Jia, S.; Wang, X.; Cheng, W.H.; Sengupta, S.; et al. Prestin-based outer hair cell motility is necessary for mammalian cochlear amplification. *Neuron* **2008**, *58*, 333–339. [[CrossRef](#)] [[PubMed](#)]
7. Everett, L.A.; Glaser, B.; Beck, J.C.; Idol, J.R.; Buchs, A.; Heyman, M.; Adawi, F.; Hazani, E.; Nassir, E.; Baxevarian, A.D.; et al. Pendred syndrome is caused by mutations in a putative sulphate transporter gene (PDS). *Nat. Genet.* **1997**, *17*, 411–422. [[CrossRef](#)] [[PubMed](#)]
8. Pryor, S.P.; Madeo, A.C.; Reynolds, J.C.; Sarlis, N.J.; Arnos, K.S.; Nance, W.E.; Yang, Y.; Zalewski, C.K.; Brewer, C.C.; Butman, J.A.; et al. SLC26A4/PDS genotype-phenotype correlation in hearing loss with enlargement of the vestibular aqueduct (EVA): Evidence that Pendred syndrome and non-syndromic EVA are distinct clinical and genetic entities. *J. Med. Genet.* **2005**, *42*, 159–165. [[CrossRef](#)] [[PubMed](#)]
9. Stenson, P.D.; Mort, M.; Ball, E.V.; Chapman, M.; Evans, K.; Azevedo, L.; Hayden, M.; Heywood, S.; Millar, D.S.; Phillips, A.D.; et al. The Human Gene Mutation Database (HGMD(R)): Optimizing its use in a clinical diagnostic or research setting. *Hum. Genet.* **2020**, *139*, 1197–1207. [[CrossRef](#)] [[PubMed](#)]
10. Wasano, K.; Takahashi, S.; Rosenberg, S.K.; Kojima, T.; Mutai, H.; Matsunaga, T.; Ogawa, K.; Homma, K. Systematic quantification of the anion transport function of pendrin (SLC26A4) and its disease-associated variants. *Hum. Mutat.* **2020**, *41*, 316–331. [[CrossRef](#)] [[PubMed](#)]
11. Takahashi, S.; Cheatham, M.A.; Zheng, J.; Homma, K. The R130S mutation significantly affects the function of prestin, the outer hair cell motor protein. *J. Mol. Med.* **2016**, *94*, 1053–1062. [[CrossRef](#)] [[PubMed](#)]
12. Takahashi, S.; Zhou, Y.; Cheatham, M.A.; Homma, K. The pathogenic roles of the p.R130S prestin variant in DFNB61 hearing loss. *bioRxiv* **2023**. [[CrossRef](#)]
13. Oza, A.M.; DiStefano, M.T.; Hemphill, S.E.; Cushman, B.J.; Grant, A.R.; Siegert, R.K.; Shen, J.; Chapin, A.; Boczek, N.J.; Schimmenti, L.A.; et al. Expert specification of the ACMG/AMP variant interpretation guidelines for genetic hearing loss. *Hum. Mutat.* **2018**, *39*, 1593–1613. [[CrossRef](#)] [[PubMed](#)]
14. Ashmore, J.F. Forward and reverse transduction in the mammalian cochlea. *Neurosci. Res. Suppl.* **1990**, *12*, S39–S50. [[CrossRef](#)] [[PubMed](#)]
15. Santos-Sacchi, J. Reversible inhibition of voltage-dependent outer hair cell motility and capacitance. *J. Neurosci.* **1991**, *11*, 3096–3110. [[CrossRef](#)] [[PubMed](#)]
16. Cheng, J.; Novati, G.; Pan, J.; Bycroft, C.; Zemgulyte, A.; Applebaum, T.; Pritzel, A.; Wong, L.H.; Zielinski, M.; Sargeant, T.; et al. Accurate proteome-wide missense variant effect prediction with AlphaMissense. *Science* **2023**, *381*, eadg7492. [[CrossRef](#)] [[PubMed](#)]
17. Liu, Q.; Zhang, X.; Huang, H.; Chen, Y.; Wang, F.; Hao, A.; Zhan, W.; Mao, Q.; Hu, Y.; Han, L.; et al. Asymmetric pendrin homodimer reveals its molecular mechanism as anion exchanger. *Nat. Commun.* **2023**, *14*, 3012. [[CrossRef](#)]
18. Ge, J.; Elferich, J.; Dehghani-Ghahnaviyeh, S.; Zhao, Z.; Meadows, M.; von Gersdorff, H.; Tajkhorshid, E.; Gouaux, E. Molecular mechanism of prestin electromotive signal amplification. *Cell* **2021**, *184*, 4669–4679.e4613. [[CrossRef](#)]
19. Bavi, N.; Clark, M.D.; Contreras, G.F.; Shen, R.; Reddy, B.G.; Milewski, W.; Perozo, E. The conformational cycle of prestin underlies outer-hair cell electromotility. *Nature* **2021**, *600*, 553–558. [[CrossRef](#)]
20. Butan, C.; Song, Q.; Bai, J.P.; Tan, W.J.T.; Navaratnam, D.; Santos-Sacchi, J. Single particle cryo-EM structure of the outer hair cell motor protein prestin. *Nat. Commun.* **2022**, *13*, 290. [[CrossRef](#)]

21. Futamata, H.; Fukuda, M.; Umeda, R.; Yamashita, K.; Tomita, A.; Takahashi, S.; Shikakura, T.; Hayashi, S.; Kusakizako, T.; Nishizawa, T.; et al. Cryo-EM structures of thermostabilized prestin provide mechanistic insights underlying outer hair cell electromotility. *Nat. Commun.* **2022**, *13*, 6208. [[CrossRef](#)]
22. Tippett, D.N.; Breen, C.; Butler, S.J.; Sawicka, M.; Dutzler, R. Structural and functional properties of the transporter SLC26A6 reveal mechanism of coupled anion exchange. *eLife* **2023**, *12*, RP87178. [[CrossRef](#)]
23. Walter, J.D.; Sawicka, M.; Dutzler, R. Cryo-EM structures and functional characterization of murine Slc26a9 reveal mechanism of uncoupled chloride transport. *eLife* **2019**, *8*, e46986. [[CrossRef](#)]
24. Chi, X.; Jin, X.; Chen, Y.; Lu, X.; Tu, X.; Li, X.; Zhang, Y.; Lei, J.; Huang, J.; Huang, Z.; et al. Structural insights into the gating mechanism of human SLC26A9 mediated by its C-terminal sequence. *Cell Discov.* **2020**, *6*, 55. [[CrossRef](#)]
25. Huang, B.; Han, M.; Wang, G.; Huang, S.; Zeng, J.; Yuan, Y.; Dai, P. Genetic mutations in non-syndromic deafness patients in Hainan Province have a different mutational spectrum compared to patients from Mainland China. *Int. J. Pediatr. Otorhinolaryngol.* **2018**, *108*, 49–54. [[CrossRef](#)]
26. Carvalho, S.; Grangeiro, C.H.P.; Picanco-Albuquerque, C.G.; Dos Anjos, T.O.; De Molfetta, G.A.; Silva, W.A., Jr.; Ferraz, V.E.F. Contribution of SLC26A4 to the molecular diagnosis of nonsyndromic prelingual sensorineural hearing loss in a Brazilian cohort. *BMC Res. Notes* **2018**, *11*, 546. [[CrossRef](#)]
27. Rendtorff, N.D.; Schrijver, I.; Lodahl, M.; Rodriguez-Paris, J.; Johnsen, T.; Hansen, E.C.; Nickelsen, L.A.; Tumer, Z.; Fagerheim, T.; Wetke, R.; et al. SLC26A4 mutation frequency and spectrum in 109 Danish Pendred syndrome/DFNB4 probands and a report of nine novel mutations. *Clin. Genet.* **2013**, *84*, 388–391. [[CrossRef](#)]
28. Turner, T.N.; Wilfert, A.B.; Bakken, T.E.; Bernier, R.A.; Pepper, M.R.; Zhang, Z.; Torene, R.I.; Retterer, K.; Eichler, E.E. Sex-Based Analysis of De Novo Variants in Neurodevelopmental Disorders. *Am. J. Hum. Genet.* **2019**, *105*, 1274–1285. [[CrossRef](#)] [[PubMed](#)]
29. Elsayed, O.; Al-Shamsi, A. Mutation spectrum of non-syndromic hearing loss in the UAE, a retrospective cohort study and literature review. *Mol. Genet. Genomic Med.* **2022**, *10*, e2052. [[CrossRef](#)] [[PubMed](#)]
30. Coyle, B.; Reardon, W.; Herbrick, J.A.; Tsui, L.C.; Gausden, E.; Lee, J.; Coffey, R.; Grueters, A.; Grossman, A.; Phelps, P.D.; et al. Molecular analysis of the PDS gene in Pendred syndrome. *Hum. Mol. Genet.* **1998**, *7*, 1105–1112. [[CrossRef](#)] [[PubMed](#)]
31. Koohiyan, M.; Hashemzadeh-Chaleshtori, M.; Tabatabaiefar, M.A. Molecular diagnosis of SLC26A4-related hereditary hearing loss in a group of patients from two provinces of Iran. *Intractable Rare Dis. Res.* **2021**, *10*, 23–30. [[CrossRef](#)] [[PubMed](#)]
32. Wu, C.C.; Yeh, T.H.; Chen, P.J.; Hsu, C.J. Prevalent SLC26A4 mutations in patients with enlarged vestibular aqueduct and/or Mondini dysplasia: A unique spectrum of mutations in Taiwan, including a frequent founder mutation. *Laryngoscope* **2005**, *115*, 1060–1064. [[CrossRef](#)]
33. Sakuma, N.; Moteki, H.; Takahashi, M.; Nishio, S.Y.; Arai, Y.; Yamashita, Y.; Oridate, N.; Usami, S. An effective screening strategy for deafness in combination with a next-generation sequencing platform: A consecutive analysis. *J. Hum. Genet.* **2016**, *61*, 253–261. [[CrossRef](#)] [[PubMed](#)]
34. Ladsous, M.; Vlaeminck-Guillem, V.; Dumur, V.; Vincent, C.; Dubrulle, F.; Dhaenens, C.M.; Wemeau, J.L. Analysis of the thyroid phenotype in 42 patients with Pendred syndrome and nonsyndromic enlargement of the vestibular aqueduct. *Thyroid.* **2014**, *24*, 639–648. [[CrossRef](#)]
35. Albert, S.; Blons, H.; Jonard, L.; Feldmann, D.; Chauvin, P.; Loundon, N.; Sergent-Allaoui, A.; Houang, M.; Joannard, A.; Schmerber, S.; et al. SLC26A4 gene is frequently involved in nonsyndromic hearing impairment with enlarged vestibular aqueduct in Caucasian populations. *Eur. J. Hum. Genet.* **2006**, *14*, 773–779. [[CrossRef](#)] [[PubMed](#)]
36. Blons, H.; Feldmann, D.; Duval, V.; Messaz, O.; Denoyelle, F.; Loundon, N.; Sergout-Allaoui, A.; Houang, M.; Duriez, F.; Lacombe, D.; et al. Screening of SLC26A4 (PDS) gene in Pendred’s syndrome: A large spectrum of mutations in France and phenotypic heterogeneity. *Clin. Genet.* **2004**, *66*, 333–340. [[CrossRef](#)] [[PubMed](#)]
37. Wang, Q.J.; Zhao, Y.L.; Rao, S.Q.; Guo, Y.F.; Yuan, H.; Zong, L.; Guan, J.; Xu, B.C.; Wang, D.Y.; Han, M.K.; et al. A distinct spectrum of SLC26A4 mutations in patients with enlarged vestibular aqueduct in China. *Clin. Genet.* **2007**, *72*, 245–254. [[CrossRef](#)] [[PubMed](#)]
38. Park, H.J.; Shaukat, S.; Liu, X.Z.; Hahn, S.H.; Naz, S.; Ghosh, M.; Kim, H.N.; Moon, S.K.; Abe, S.; Tukamoto, K.; et al. Origins and frequencies of SLC26A4 (PDS) mutations in east and south Asians: Global implications for the epidemiology of deafness. *J. Med. Genet.* **2003**, *40*, 242–248. [[CrossRef](#)]
39. Miyagawa, M.; Nishio, S.Y.; Usami, S.; Deafness Gene Study, C. Mutation spectrum and genotype-phenotype correlation of hearing loss patients caused by SLC26A4 mutations in the Japanese: A large cohort study. *J. Hum. Genet.* **2014**, *59*, 262–268. [[CrossRef](#)]
40. Hutchin, T.; Coy, N.N.; Conlon, H.; Telford, E.; Bromelow, K.; Blyndon, D.; Taylor, G.; Coghill, E.; Brown, S.; Trembath, R.; et al. Assessment of the genetic causes of recessive childhood non-syndromic deafness in the UK—Implications for genetic testing. *Clin. Genet.* **2005**, *68*, 506–512. [[CrossRef](#)]
41. Reardon, W.; CF, O.M.; Trembath, R.; Jan, H.; Phelps, P.D. Enlarged vestibular aqueduct: A radiological marker of pendred syndrome, and mutation of the PDS gene. *QJM* **2000**, *93*, 99–104. [[CrossRef](#)] [[PubMed](#)]
42. Choi, B.Y.; Stewart, A.K.; Madeo, A.C.; Pryor, S.P.; Lenhard, S.; Kittles, R.; Eisenman, D.; Kim, H.J.; Niparko, J.; Thomsen, J.; et al. Hypo-functional SLC26A4 variants associated with nonsyndromic hearing loss and enlargement of the vestibular aqueduct: Genotype-phenotype correlation or coincidental polymorphisms? *Hum. Mutat.* **2009**, *30*, 599–608. [[CrossRef](#)] [[PubMed](#)]

43. Wen, C.; Wang, S.; Zhao, X.; Wang, X.; Wang, X.; Cheng, X.; Huang, L. Mutation analysis of the SLC26A4 gene in three Chinese families. *Biosci. Trends* **2019**, *13*, 441–447. [[CrossRef](#)]
44. Landa, P.; Differ, A.M.; Rajput, K.; Jenkins, L.; Bitner-Glindzicz, M. Lack of significant association between mutations of KCNJ10 or FOXI1 and SLC26A4 mutations in Pendred syndrome/enlarged vestibular aqueducts. *BMC Med. Genet.* **2013**, *14*, 85. [[CrossRef](#)]
45. Zhao, J.; Yuan, Y.; Huang, S.; Huang, B.; Cheng, J.; Kang, D.; Wang, G.; Han, D.; Dai, P. KCNJ10 may not be a contributor to nonsyndromic enlargement of vestibular aqueduct (NSEVA) in Chinese subjects. *PLoS ONE* **2014**, *9*, e108134. [[CrossRef](#)]
46. Chen, D.Y.; Chen, X.W.; Jin, X.; Zuo, J.; Wei, C.G.; Cao, K.L.; Fang, F.D. Screening of SLC26A4 (PDS) gene mutation in cochlear implant recipients with inner ear malformation. *Zhonghua Yi Xue Za Zhi* **2007**, *87*, 2820–2824.
47. Van Hauwe, P.; Everett, L.A.; Coucke, P.; Scott, D.A.; Kraft, M.L.; Ris-Stalpers, C.; Bolder, C.; Otten, B.; de Vijlder, J.J.; Dietrich, N.L.; et al. Two frequent missense mutations in Pendred syndrome. *Hum. Mol. Genet.* **1998**, *7*, 1099–1104. [[CrossRef](#)] [[PubMed](#)]
48. Chai, Y.; Huang, Z.; Tao, Z.; Li, X.; Li, L.; Li, Y.; Wu, H.; Yang, T. Molecular etiology of hearing impairment associated with nonsyndromic enlarged vestibular aqueduct in East China. *Am. J. Med. Genet. A* **2013**, *161*, 2226–2233. [[CrossRef](#)]
49. Gonzalez Trevino, O.; Karamanoglu Arseven, O.; Ceballos, C.J.; Vives, V.I.; Ramirez, R.C.; Gomez, V.V.; Medeiros-Neto, G.; Kopp, P. Clinical and molecular analysis of three Mexican families with Pendred’s syndrome. *Eur. J. Endocrinol.* **2001**, *144*, 585–593. [[CrossRef](#)]
50. Courtmans, I.; Mancilla, V.; Ligny, C.; Hilbert, P.; Mansbach, A.L.; Van Maldergem, L. Clinical findings and PDS mutations in 15 patients with hearing loss and dilatation of the vestibular aqueduct. *J. Laryngol. Otol.* **2007**, *121*, 312–317. [[CrossRef](#)]
51. Ji, Y.B.; Han, D.Y.; Wang, D.Y.; Zhou, Y.; Zhao, C.; Wang, H.; Lan, L.; Wang, Q.J. Evaluation of deaf-mute patients with sensitive deafness gene screening in Shandong province. *Zhonghua Yi Xue Za Zhi* **2009**, *89*, 2531–2535.
52. Pera, A.; Villamar, M.; Vinuela, A.; Gandia, M.; Meda, C.; Moreno, F.; Hernandez-Chico, C. A mutational analysis of the SLC26A4 gene in Spanish hearing-impaired families provides new insights into the genetic causes of Pendred syndrome and DFNB4 hearing loss. *Eur. J. Hum. Genet.* **2008**, *16*, 888–896. [[CrossRef](#)]
53. Yuan, Y.Y.; Dai, P.; Zhu, Q.W.; Kang, D.Y.; Huang, D.L. Sequencing analysis of whole SLC26A4 gene related to IVS7-2A > G mutation in 1552 moderate to profound sensorineural hearing loss patients in China. *Zhonghua Er Bi Yan Hou Tou Jing Wai Ke Za Zhi* **2009**, *44*, 449–454. [[PubMed](#)]
54. Sloan-Heggen, C.M.; Bierer, A.O.; Shearer, A.E.; Kolbe, D.L.; Nishimura, C.J.; Frees, K.L.; Ephraim, S.S.; Shibata, S.B.; Booth, K.T.; Campbell, C.A.; et al. Comprehensive genetic testing in the clinical evaluation of 1119 patients with hearing loss. *Hum. Genet* **2016**, *135*, 441–450. [[CrossRef](#)]
55. Scott, D.A.; Wang, R.; Kreman, T.M.; Andrews, M.; McDonald, J.M.; Bishop, J.R.; Smith, R.J.; Karniski, L.P.; Sheffield, V.C. Functional differences of the PDS gene product are associated with phenotypic variation in patients with Pendred syndrome and non-syndromic hearing loss (DFNB4). *Hum. Mol. Genet.* **2000**, *9*, 1709–1715. [[CrossRef](#)] [[PubMed](#)]
56. Yoon, J.S.; Park, H.J.; Yoo, S.Y.; Namkung, W.; Jo, M.J.; Koo, S.K.; Park, H.Y.; Lee, W.S.; Kim, K.H.; Lee, M.G. Heterogeneity in the processing defect of SLC26A4 mutants. *J. Med. Genet.* **2008**, *45*, 411–419. [[CrossRef](#)]
57. Ishihara, K.; Okuyama, S.; Kumano, S.; Iida, K.; Hamana, H.; Murakoshi, M.; Kobayashi, T.; Usami, S.; Ikeda, K.; Haga, Y.; et al. Salicylate restores transport function and anion exchanger activity of missense pendrin mutations. *Hear. Res.* **2010**, *270*, 110–118. [[CrossRef](#)]
58. Gillam, M.P.; Bartolone, L.; Kopp, P.; Benvenga, S. Molecular analysis of the PDS gene in a nonconsanguineous Sicilian family with Pendred’s syndrome. *Thyroid.* **2005**, *15*, 734–741. [[CrossRef](#)]
59. Taylor, J.P.; Metcalfe, R.A.; Watson, P.F.; Weetman, A.P.; Trembath, R.C. Mutations of the PDS gene, encoding pendrin, are associated with protein mislocalization and loss of iodide efflux: Implications for thyroid dysfunction in Pendred syndrome. *J. Clin. Endocrinol. Metab.* **2002**, *87*, 1778–1784. [[CrossRef](#)] [[PubMed](#)]
60. de Moraes, V.C.S.; Bernardinelli, E.; Zocal, N.; Fernandez, J.A.; Nofziger, C.; Castilho, A.M.; Sartorato, E.L.; Paulmichl, M.; Dossena, S. Reduction of Cellular Expression Levels Is a Common Feature of Functionally Affected Pendrin (SLC26A4) Protein Variants. *Mol. Med.* **2016**, *22*, 41–53. [[CrossRef](#)]
61. Pera, A.; Dossena, S.; Rodighiero, S.; Gandia, M.; Botta, G.; Meyer, G.; Moreno, F.; Nofziger, C.; Hernandez-Chico, C.; Paulmichl, M. Functional assessment of allelic variants in the SLC26A4 gene involved in Pendred syndrome and nonsyndromic EVA. *Proc. Natl. Acad. Sci. USA* **2008**, *105*, 18608–18613. [[CrossRef](#)]
62. Han, J.J.; Nguyen, P.D.; Oh, D.Y.; Han, J.H.; Kim, A.R.; Kim, M.Y.; Park, H.R.; Tran, L.H.; Dung, N.H.; Koo, J.W.; et al. Elucidation of the unique mutation spectrum of severe hearing loss in a Vietnamese pediatric population. *Sci. Rep.* **2019**, *9*, 1604. [[CrossRef](#)]
63. Cardenas, R.; Prinsley, P.; Philpott, C.; Bhutta, M.F.; Wilson, E.; Brewer, D.S.; Jennings, B.A. Whole exome sequencing study identifies candidate loss of function variants and locus heterogeneity in familial cholesteatoma. *PLoS ONE* **2023**, *18*, e0272174. [[CrossRef](#)]
64. Mutai, H.; Suzuki, N.; Shimizu, A.; Torii, C.; Namba, K.; Morimoto, N.; Kudoh, J.; Kaga, K.; Kosaki, K.; Matsunaga, T. Diverse spectrum of rare deafness genes underlies early-childhood hearing loss in Japanese patients: A cross-sectional, multi-center next-generation sequencing study. *Orphanet J. Rare Dis.* **2013**, *8*, 172. [[CrossRef](#)]
65. Toth, T.; Deak, L.; Fazakas, F.; Zheng, J.; Muszbek, L.; Sziklai, I. A new mutation in the human pres gene and its effect on prestin function. *Int. J. Mol. Med.* **2007**, *20*, 545–550. [[CrossRef](#)] [[PubMed](#)]

66. Zhou, X.; Feliciano, P.; Shu, C.; Wang, T.; Astrovskaya, I.; Hall, J.B.; Obiajulu, J.U.; Wright, J.R.; Murali, S.C.; Xu, S.X.; et al. Integrating de novo and inherited variants in 42,607 autism cases identifies mutations in new moderate-risk genes. *Nat. Genet.* **2022**, *54*, 1305–1319. [[CrossRef](#)]
67. Morgan, A.; Lenarduzzi, S.; Cappellani, S.; Pecile, V.; Morgutti, M.; Orzan, E.; Ghiselli, S.; Ambrosetti, U.; Brumat, M.; Gajendrarao, P.; et al. Genomic Studies in a Large Cohort of Hearing Impaired Italian Patients Revealed Several New Alleles, a Rare Case of Uniparental Disomy (UPD) and the Importance to Search for Copy Number Variations. *Front. Genet.* **2018**, *9*, 681. [[CrossRef](#)] [[PubMed](#)]
68. Koire, A.; Katsonis, P.; Kim, Y.W.; Buchovecky, C.; Wilson, S.J.; Lichtarge, O. A method to delineate de novo missense variants across pathways prioritizes genes linked to autism. *Sci. Transl. Med.* **2021**, *13*, eabc1739. [[CrossRef](#)]
69. Brandes, N.; Weissbrod, O.; Linial, M. Open problems in human trait genetics. *Genome Biol.* **2022**, *23*, 131. [[CrossRef](#)] [[PubMed](#)]
70. Richards, S.; Aziz, N.; Bale, S.; Bick, D.; Das, S.; Gastier-Foster, J.; Grody, W.W.; Hegde, M.; Lyon, E.; Spector, E.; et al. Standards and guidelines for the interpretation of sequence variants: A joint consensus recommendation of the American College of Medical Genetics and Genomics and the Association for Molecular Pathology. *Genet. Med.* **2015**, *17*, 405–424. [[CrossRef](#)]
71. Livesey, B.J.; Marsh, J.A. Interpreting protein variant effects with computational predictors and deep mutational scanning. *Dis. Model. Mech.* **2022**, *15*, dmm049510. [[CrossRef](#)]
72. Tollefson, M.R.; Gogal, R.A.; Weaver, A.M.; Schaefer, A.M.; Marini, R.J.; Azaiez, H.; Kolbe, D.L.; Wang, D.; Weaver, A.E.; Casavant, T.L.; et al. Assessing variants of uncertain significance implicated in hearing loss using a comprehensive deafness proteome. *Hum. Genet.* **2023**, *142*, 819–834. [[CrossRef](#)]
73. Fowler, D.M.; Adams, D.J.; Gloyn, A.L.; Hahn, W.C.; Marks, D.S.; Muffley, L.A.; Neal, J.T.; Roth, F.P.; Rubin, A.F.; Starita, L.M.; et al. An Atlas of Variant Effects to understand the genome at nucleotide resolution. *Genome Biol.* **2023**, *24*, 147. [[CrossRef](#)] [[PubMed](#)]
74. Tabet, D.; Parikh, V.; Mali, P.; Roth, F.P.; Claussnitzer, M. Scalable Functional Assays for the Interpretation of Human Genetic Variation. *Annu. Rev. Genet.* **2022**, *56*, 441–465. [[CrossRef](#)] [[PubMed](#)]
75. Keller, J.P.; Homma, K.; Duan, C.; Zheng, J.; Cheatham, M.A.; Dallos, P. Functional regulation of the SLC26-family protein prestin by calcium/calmodulin. *J. Neurosci.* **2014**, *34*, 1325–1332. [[CrossRef](#)] [[PubMed](#)]
76. Xu, J.; Barone, S.; Varasteh Kia, M.; Holliday, L.S.; Zahedi, K.; Soleimani, M. Identification of IQGAP1 as a SLC26A4 (Pendrin)-Binding Protein in the Kidney. *Front. Mol. Biosci.* **2022**, *9*, 874186. [[CrossRef](#)]
77. Zheng, J.; Du, G.G.; Matsuda, K.; Orem, A.; Aguinaga, S.; Deak, L.; Navarrete, E.; Madison, L.D.; Dallos, P. The C-terminus of prestin influences nonlinear capacitance and plasma membrane targeting. *J. Cell Sci.* **2005**, *118*, 2987–2996. [[CrossRef](#)]
78. Zheng, L.; Zheng, J.; Whitlon, D.S.; Garcia-Anoveros, J.; Bartles, J.R. Targeting of the hair cell proteins cadherin 23, harmonin, myosin XVa, espin, and prestin in an epithelial cell model. *J. Neurosci.* **2010**, *30*, 7187–7201. [[CrossRef](#)]
79. Royaux, I.E.; Suzuki, K.; Mori, A.; Katoh, R.; Everett, L.A.; Kohn, L.D.; Green, E.D. Pendrin, the protein encoded by the Pendred syndrome gene (PDS), is an apical porter of iodide in the thyroid and is regulated by thyroglobulin in FRTL-5 cells. *Endocrinology* **2000**, *141*, 839–845. [[CrossRef](#)]
80. Wangemann, P.; Itza, E.M.; Albrecht, B.; Wu, T.; Jabba, S.V.; Maganti, R.J.; Lee, J.H.; Everett, L.A.; Wall, S.M.; Royaux, I.E.; et al. Loss of KCNJ10 protein expression abolishes endocochlear potential and causes deafness in Pendred syndrome mouse model. *BMC Med.* **2004**, *2*, 30. [[CrossRef](#)]
81. Santos-Sacchi, J.; Kakehata, S.; Takahashi, S. Effects of membrane potential on the voltage dependence of motility-related charge in outer hair cells of the guinea-pig. *J. Physiol.* **1998**, *510 Pt 1*, 225–235. [[CrossRef](#)] [[PubMed](#)]
82. Takahashi, S.; Zhou, Y.; Kojima, T.; Cheatham, M.A.; Homma, K. Prestin's fast motor kinetics is essential for mammalian cochlear amplification. *Proc. Natl. Acad. Sci. USA* **2023**, *120*, e2217891120. [[CrossRef](#)] [[PubMed](#)]

Disclaimer/Publisher's Note: The statements, opinions and data contained in all publications are solely those of the individual author(s) and contributor(s) and not of MDPI and/or the editor(s). MDPI and/or the editor(s) disclaim responsibility for any injury to people or property resulting from any ideas, methods, instructions or products referred to in the content.